Defence Technology xxx (xxxx) xxx

Contents lists available at ScienceDirect

Defence Technology

journal homepage: www.keaipublishing.com/en/journals/defence-technology

Isogeometric analysis for free vibration of bidirectional functionally graded plates in the fluid medium

Quoc-Hoa Pham [a], Phu-Cuong Nguyen [a], Van Ke Tran [b], Trung Nguyen-Thoi [c, d, *]

[a] Faculty of Civil Engineering, Ho Chi Minh City Open University, Ho Chi Minh City, Viet Nam
[b] Faculty of Mechanical Engineering, Le Quy Don Technical University, Hanoi, Viet Nam
[c] Division of Computational Mathematics and Engineering, Institute for Computational Science, Ton Duc Thang University, Ho Chi Minh City, Viet Nam
[d] Faculty of Civil Engineering, Ton Duc Thang University, Ho Chi Minh City, Viet Nam

ARTICLE INFO

Article history:
Received 1 July 2021
Received in revised form
16 August 2021
Accepted 8 September 2021
Available online xxx

Keywords:
Contact plate-fluid
Refined quasi 3D plate theory
Mori -Tanaka model
Isogeometric analysis
Bidirectional functionally graded plate

ABSTRACT

This paper for first time proposes an isogeometric analysis (IGA) for free vibration response of bidirectional functionally graded (BDFG) rectangular plates in the fluid medium. Material properties of the BDFG plate change in both the thickness and length directions via power-law distributions and Mori-Tanaka model. The governing equation of motion of BDFG plate in the fluid-plate system is formulated basing on Hamilton's principle and the refined quasi three-dimensional (3D) plate theory with improved function $f(z)$. The fluid velocity potential is derived from the boundary conditions of the fluid-plate system and is used to determine the added mass. The discrete system of equations is derived from the Galerkin weak form and numerically analyzed by IGA. The accuracy and reliability of the proposed solutions are verified by comparing the obtained results with those published in the literature. Moreover, the effects of the various parameters such as the interaction boundary condition, geometric parameter, submerged depth of plate, fluid density, fluid level, and the material volume control coefficients on the free vibration behavior of BDFG plate in the fluid medium are investigated in detail. Some major findings regarding the numerical results are withdrawn in conclusions.

1. Introduction

In recent years, thanks to superior properties such as lightweight, high stiffness, capable of resisting high-temperature environments or extremely large temperature gradients, the functionally graded material (FGM) has been widely used in many engineering fields including mechanical, automotive, aero-space, civil engineering, and defense industry. Due to the above-mentioned advantages and ample applications, the analysis of the mechanical behavior of the structures using the FGM has been investigated worldwide by many investigators [1–3]. For example, Tahir et al. [4,5] and Menasria et al. [6] proposed the simple four-unknown theory to investigate the behavior of FG porous plates. Chakraverty and Pradhan [7] developed the Rayleigh-Ritz method basing on classical plate theory to investigate the free vibration of functionally graded plates with various boundary conditions. Zaoui et al. [8] used the novel shear strain shape function based on 2D and quasi 3D theories to study the free vibration of FGM plates resting on elastic foundations. Karami et al. [9] applied the second-order shear deformation theory to analyze the dynamic and buckling response of functionally graded carbon nanotube-reinforced composite plates on elastic foundation. Also, studying the FG plates resting on elastic foundation using an analytical approach was introduced in documents [10–12]. Hachemi et al. [13] developed a new refined quasi-3D shear deformation theory and the concept of the neutral surface position to investigate the bending behavior of FG plates. Bakoura et al. [14] proposed a higher order shear deformation theory (HSDT) in conjunction with the stress function method to study the buckling behavior of FG plates. Bekkaye et al. [15] used the refined trigonometric shear deformation theory to analyze the mechanical response of FG porous plates. Rezaei et al. [16] presented the free vibration of FG plates based on the simple first-order shear deformation theory. Li et al. [17] proposed the new five-variable shear deformation theory to analyze the static

* Corresponding author. Division of Computational Mathematics and Engineering, Institute for Computational Science, Ton Duc Thang University, Ho Chi Minh City, Viet Nam.
E-mail address: nguyenthoitrung@tdtu.edu.vn (T. Nguyen-Thoi).
Peer review under responsibility of China Ordnance Society

https://doi.org/10.1016/j.dt.2021.09.006

Please cite this article as: Q.-H. Pham, P.-C. Nguyen, V.K. Tran *et al.*, Isogeometric analysis for free vibration of bidirectional functionally graded plates in the fluid medium, Defence Technology, https://doi.org/10.1016/j.dt.2021.09.006

bending behavior of FG plates. Nguyen et al. [18] developed the polygonal finite element method to investigate the static bending and vibration responses of FG porous plates with graphene platelets reinforcement. Kumar et al. [19] used the nonlinear FEM to study the vibration and transient response of FGP skew plates. Recently, Tran et al. [20–22] used the edge-based smoothed finite element method to study the static bending, vibration and dynamic behavior of FG porous plates. Also, Pham et al. [23] investigated the nonlinear static bending response of FGM shell and Tran et al. [24] studied the static and vibration behaviors of FG porous plates reinforced by graphene platelets.

Nevertheless, the structures made from the transverse FGMs or axial FGMs are not efficient enough for the applications in the aerospace, defense industry, or nuclear reactors when the temperature distributes differently along different directions. Thus, the multi-directional FGMs (MDFGMs) was proposed to meet these demands. To study the properties of MDFGMs, Karamanli and Vo [25] investigated the static bending behavior of two-dimensional FG microbeams under uniformly distributed loads using the quasi-3D model and modified couple stress theory. Li et al. [26] proposed the isogeometric analysis (IGA) based on the first-order shear deformation theory (FSDT) to analyze the static bending, free vibration and buckling responses of bi-directional FG porous plates. Also, Lieu et al. [27,28] employed the IGA based on NURBS to investigate the static bending, vibration and buckling responses of bi-directional FG plates and variable thickness plates. Wu and Yu [29] developed a finite annular prism method to analyze the free vibration response of bi-directional FG annular plates.

The structures in the fluid medium have been applied in various fields such as nuclear, ocean, naval engineering and defense industry. Therefore, a clear understanding of the behavior of the structures in the fluid medium is necessary and has been studied widely by many researchers. Cho et al. [30,31] proposed an analytical approach to study the free vibration and forced vibration of plates and stiffened panels contact with fluid on one side. Hashemi et al. [32] developed the Ritz method to analyze the free vibration of vertical plates resting on the foundation in contact with fluid on one side. Watts et al. [33] proposed the semi-analytical method that relied on the Galerkin to investigate the vibration response of the non-rectangular bottom of tanks filling with liquid. Bendahmane et al. [34] employed the hierarchical finite element method based on the higher-order shear deformation theory to study the natural frequency of composite plates with variable stiffness submerged in fluid. Khorshidi et al. [35–37] used the Rayleigh-Ritz method with finite Fourier series to determine the natural frequencies of square plates in contact with a bounded fluid. In this study, they examined different materials of plates such as isotropic, laminate composite, and functionally graded materials.

The isogeometric analysis (IGA) proposed by Hughes et al. [38], which combines computer-aided design and finite element analysis, has been developed by many researchers for its advantages and effectiveness. The essential idea of the isogeometric analysis is to employ the same basis functions to exactly describe the geometry domain, as well as to approximate the unknown fields. Since the geometry is exactly modelled and the number of unknown terms does not increase, it is expected that the IGA would yield more accurate results with lower computational cost for plate problems using HSDT or refined higher-order shear deformation plate theory (RPT) in the comparison with other numerical methods such as finite trip method, finite element method, or meshfree method, etc. The IGA has been developed for analyzing many different structures such as analysis beams [39–46], plates [47–55] and shells [56–63]. Most of the works have given the conclusion that the IGA has high accuracy and can be extended relatively easily for complex structures. In particular, thanks to satisfying higher-order derivatives of NURBS functions and the suitability to use the elasticity nonlocal theory, the IGA has been applied in many nanostructures such as nanobeams [64,65], nanoplates [66–74] and nanoshells [75,76]. However, based on the updated knowledge of the authors, the analysis of the structures in the fluid medium by using the IGA is still limited.

As observed from the above literature reviews to the authors' best knowledge, the investigation on the free vibration of the FGM plates in the fluid medium using the IGA has not yet been studied. This paper is hence performed to fill in this research gap by proposing an IGA for free vibration analysis of bi-directional functionally graded (BDFG) rectangular plates in the fluid medium. The plates are considered in the fluid medium including the cases of the plate in horizontal or vertical positions and the plate in full or partial contact with fluid. The material properties are assumed to change continuously in both the thickness and length directions according to a power-law distribution and using Mori-Tanaka model. Hamilton's principle and the refined quasi three-dimensional (3D) plate theory with improved function $f(z)$ are used to set up the governing equation of the BDFG plate in the fluid medium. The discrete system of equations is derived from the Galerkin weak form and numerically analyzed by the IGA. The obtained numerical results are compared with other published works in literature to demonstrate the accuracy and reliability of the proposed method. In addition, the influences of the various parameters such as the interaction boundary condition, geometric parameter, and material volume control coefficients on the free vibration response of BDFG plates in the fluid medium are also examined. The present work helps to add physical data and laws in the design and manufacture of structures in engineering fields such as maritime and aviation. Further more, the results of present work can be applied in the defense fields such as fuel tanks, submarines, warships, underground structures in the ocean, military structures on the seas and islands, cooling areas of furnaces nuclear reactions, etc.

For the convenience of readers, the sections of the article are arranged as follows: Section 1 is a general introduction. Section 2 introduces the theoretical formulation. Section 3 presents the NURBS functions and IGA for free vibration of BDFG plates in the fluid medium. Section 4 presents the numerical results to demonstrate the accuracy and reliability of the proposed method. Finally, some major conclusions are withdrawn in Section 5.

2. Theoretical formulation

2.1. Model of bidirectional functionally graded rectangular plates

We consider a rectangular BDFG plate has the length a, the width b and the thickness h, which is made from a mixture of ceramics and metals as shown in Fig. 1. The material properties are assumed to change continuously from a top surface ($z = +h/2$) to the bottom surface ($z = -h/2$) according to a power-law distribution. The volume fraction of ceramic V_c and metal V_m varies in both the thickness and length directions according to the law of:

$$V_c = \left(\frac{1}{2}+\frac{z}{h}\right)^{p_z}\left(\frac{x}{a}\right)^{p_x}; V_m = 1 - V_c \quad (1)$$

where p_z and p_x are the non-negative axial and transverse power-law indexes, which determine the material distribution in the length and thickness directions of the plate, respectively.

Two micromechanical models, namely the Voigt model and Mori-Tanaka scheme are employed herein to evaluate the effective material properties of the BDFG plate. An effective property $P(x,z)$ such as elastic modulus and mass density evaluated by the Voigt

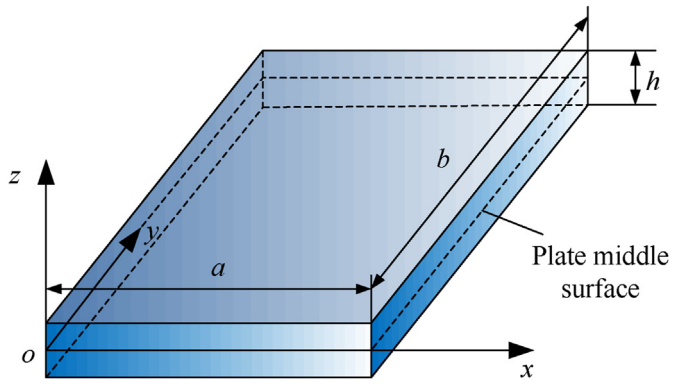

Fig. 1. Model of a bi-directional functionally graded (BDFG) rectangular plate.

model is of the form:

$$P(x,z) = P_{\mathrm{m}} + (P_{\mathrm{c}} - P_{\mathrm{m}})V_{\mathrm{c}} \tag{2}$$

where P is the effective material property such as Young's modulus E, mass density ρ, and Poisson's ratio υ; subscripts m and c denote the metallic and ceramic constituents, respectively.

According to the Mori-Tanaka scheme (Mori and Tanaka [77]), the effective bulk modulus K_{p} and shear modulus G_{p} at any point of the plate are given by:

$$K_{\mathrm{p}} = K_{\mathrm{m}} + \frac{V_{\mathrm{c}}(K_{\mathrm{c}} - K_{\mathrm{m}})}{1 + V_{\mathrm{m}}(K_{\mathrm{c}} - \mathrm{K_m})/(\mathrm{K_m} + 4G_{\mathrm{m}}/3)}$$

$$G_{\mathrm{p}} = G_{\mathrm{m}} + \frac{V_{\mathrm{c}}(G_{\mathrm{c}} - G_{\mathrm{m}})}{1 + V_{\mathrm{m}}(G_{\mathrm{c}} - G_{\mathrm{m}})/(K_{\mathrm{m}} + G_{\mathrm{m}}(9K_{\mathrm{m}} + 8G_{\mathrm{m}})/(6K_{\mathrm{m}} + 12G_{\mathrm{m}}))} \tag{3}$$

where

$$K_{\mathrm{c}} = \frac{E_{\mathrm{c}}}{3(1-\upsilon_{\mathrm{c}})}; K_{\mathrm{m}} = \frac{E_{\mathrm{m}}}{3(1-\upsilon_{\mathrm{m}})}; G_{\mathrm{c}} = \frac{E_{\mathrm{c}}}{2(1+\upsilon_{\mathrm{c}})}; G_{\mathrm{m}} = \frac{E_{\mathrm{m}}}{2(1+\upsilon_{\mathrm{c}})} \tag{4}$$

The effectiveness of Young's modulus E and Poisson's ratio υ are computed via the effective bulk modulus and shear modulus as follows.

$$E(x,z) = \frac{9K_{\mathrm{p}}G_{\mathrm{p}}}{3K_p + G_{\mathrm{p}}}; \upsilon(x,z) = \frac{3K_{\mathrm{p}} - 2G_{\mathrm{p}}}{6K_{\mathrm{p}} + 2G_{\mathrm{p}}} \tag{5}$$

Noting that the effective mass density ρ is defined by Voigt model according to Eq. (2)

$$\rho(x,z) = \rho_{\mathrm{m}} + (\rho_{\mathrm{c}} - \rho_{\mathrm{m}})V_{\mathrm{c}} \tag{6}$$

with $p_z = p_x = 2$; the Young's modulus E by Mori-Tanaka and the mass density ρ through the thickness z and the length x of BDFG plate are shown in Fig. 2.

2.2. The refined BDFG plates model

According to the refined higher-order shear deformation theory (HSDT), the displacement field of the plates by (Mantari and Soares [78]) is defined by:

$$\begin{cases} U_x(x,y,z,t) = U_0(x,y,t) + z\left(k_1\dfrac{\partial W^s}{\partial x} + k_2\dfrac{\partial \theta}{\partial x} - \dfrac{\partial W^b}{\partial x}\right) + f(z)\dfrac{\partial W^s}{\partial x} \\ U_y(x,y,z,t) = V_0(x,y,t) + z\left(k_1\dfrac{\partial W^s}{\partial y} + k_2\dfrac{\partial \theta}{\partial y} - \dfrac{\partial W^b}{\partial y}\right) + f(z)\dfrac{\partial W^s}{\partial y} \\ U_z(x,y,z,t) = W^b + W^s + g(z)\theta \end{cases} \tag{7}$$

$$k_1 = -f'\left(\frac{h}{2}\right) - 1; k_2 = -g\left(\frac{h}{2}\right) \tag{8}$$

where U_x, U_y, U_z are the displacements in the x, y, and z directions, respectively; U_0 and $V_0$are respectively the in-plane displacements of the middle surface; $W^b$and $W^s$are the bending and shear components of the transverse displacement, respectively; $f(z)$ and $g(z)$ are the functions in the form of

$$f(z) = K\frac{h}{\pi}\sin\left(\frac{\pi z}{hK}\right); g(z) = K\cos\left(\frac{\pi z}{hK}\right); \text{ with } K = \frac{\sqrt{17}}{4} \tag{9}$$

The linear strain components of the BDFG plate are written based on the displacements field in Eq. (7) by:

$$\begin{aligned} \varepsilon_{xx} &= \frac{\partial U_x}{\partial x} = \frac{\partial U_0}{\partial x} + z\left(k_1\frac{\partial^2 W^s}{\partial x^2} + k_2\frac{\partial^2 \theta}{\partial x^2} - \frac{\partial^2 W^b}{\partial x^2}\right) + f(z)\frac{\partial^2 W^s}{\partial x^2} \\ &= U_{0,x} + z\left(k_1 W^s_{,xx} + k_2\theta_{,xx} - W^b_{,xx}\right) + f(z)W^s_{,xx} \end{aligned} \tag{10}$$

$$\begin{aligned} \varepsilon_{yy} &= \frac{\partial U_y}{\partial y} = \frac{\partial V_0}{\partial y} + z\left(k_1\frac{\partial^2 W^s}{\partial y^2} + k_2\frac{\partial^2 \theta}{\partial y^2} - \frac{\partial^2 W^b}{\partial y^2}\right) + f(z)\frac{\partial^2 W^s}{\partial y^2} \\ &= V_{0,y} + z\left(k_1 W^s_{,yy} + k_2\theta_{,yy} - W^b_{,yy}\right) + f(z)W^s_{,yy} \end{aligned} \tag{11}$$

$$\varepsilon_{zz} = \frac{\partial U_z}{\partial z} = g'(z)\theta \tag{12}$$

$$\begin{aligned} \varepsilon_{xy} &= \frac{\partial U_x}{\partial y} + \frac{\partial U_y}{\partial x} = \frac{\partial U_0}{\partial y} + \frac{\partial V_0}{\partial x} + 2z\left(k_1\frac{\partial^2 W^s}{\partial x\partial y} + k_2\frac{\partial^2 \theta}{\partial x\partial y} - \frac{\partial^2 W^b}{\partial x\partial y}\right) \\ &\quad + 2f(z)\frac{\partial^2 W^s}{\partial x\partial y} = U_{0,y} + V_{0,x} + 2z\left(k_1 W^s_{,xy} + k_2\theta_{,xy} - W^b_{,xy}\right) \\ &\quad + 2f(z)W^s_{,xy} \end{aligned} \tag{13}$$

$$\begin{aligned} \gamma_{xz} &= \frac{\partial U_x}{\partial z} + \frac{\partial U_z}{\partial x} = (k_1+1)\frac{\partial W^s}{\partial x} + k_2\frac{\partial \theta}{\partial x} + g'(z)\frac{\partial \theta}{\partial x} + f'(z)\frac{\partial W^s}{\partial x} \\ &= (k_1+1)W^s_{,x} + k_2\theta_{,x} + g'(z)\theta_{,x} + f'(z)W^s_{,x} \end{aligned} \tag{14}$$

$$\begin{aligned} \gamma_{yz} &= \frac{\partial U_y}{\partial z} + \frac{\partial U_z}{\partial y} = (k_1+1)\frac{\partial W^s}{\partial y} + k_2\frac{\partial \theta}{\partial y} + g'(z)\frac{\partial \theta}{\partial y} + f'(z)\frac{\partial W^s}{\partial y} \\ &= (k_1+1)W^s_{,y} + k_2\theta_{,y} + g'(z)\theta_{,y} + f'(z)W^s_{,y} \end{aligned} \tag{15}$$

In Eqs. (14) and (15), it can be seen that the components of the transverse shear strains γ_{xz}, γ_{yz} are equal to zero on top $(z = h/2)$ and bottom surfaces $(z = -h/2)$ of the BDFG nanoplate. The strain fields of BDFG plate can be briefed in vector forms as follows:

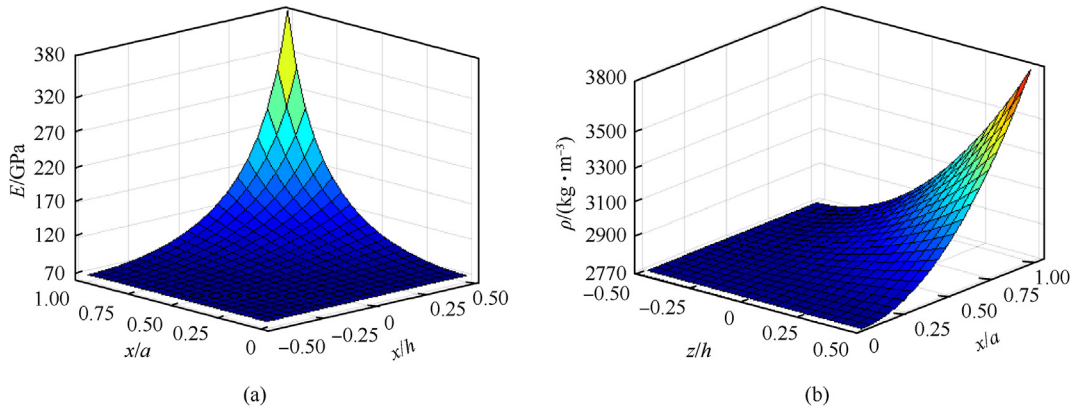

Fig. 2. Variation of Young's modulus Mori-Tanaka (a) and mass density (b) through the thickness and the length of the plate for $p_z = p_x = 2$.

$$\boldsymbol{\varepsilon}^{b} = \begin{Bmatrix} \varepsilon_{xx} \\ \varepsilon_{yy} \\ \varepsilon_{xy} \\ \varepsilon_{zz} \end{Bmatrix} = \begin{bmatrix} 1 & z & f(z) & g'(z) \end{bmatrix} \begin{Bmatrix} \boldsymbol{\varepsilon}^0 \\ \boldsymbol{\varepsilon}^1 \\ \boldsymbol{\varepsilon}^2 \\ \boldsymbol{\varepsilon}^3 \end{Bmatrix} = \begin{bmatrix} 1 & z & f(z) & g'(z) \end{bmatrix} \boldsymbol{\varepsilon};$$

$$\boldsymbol{\gamma} = \begin{Bmatrix} \gamma_{xz} \\ \gamma_{yz} \end{Bmatrix} = \begin{bmatrix} 1 & g'(z) & f'(z) \end{bmatrix} \begin{Bmatrix} \boldsymbol{\gamma}^0 \\ \boldsymbol{\gamma}^1 \\ \boldsymbol{\gamma}^2 \end{Bmatrix} \tag{16}$$

where:

$$\boldsymbol{\varepsilon} = \begin{Bmatrix} \boldsymbol{\varepsilon}^0 \\ \boldsymbol{\varepsilon}^1 \\ \boldsymbol{\varepsilon}^2 \\ \boldsymbol{\varepsilon}^3 \end{Bmatrix}; \boldsymbol{\varepsilon}^0 = \begin{Bmatrix} U_{0,x} \\ V_{0,y} \\ U_{0,y} + V_{0,x} \\ 0 \end{Bmatrix};$$

$$\boldsymbol{\varepsilon}^1 = \begin{Bmatrix} k_1 W^s_{,xx} + k_2 \theta_{,xx} - W^b_{,xx} \\ k_1 W^s_{,yy} + k_2 \theta_{,yy} - W^b_{,yy} \\ 2\left(k_1 W^s_{,xy} + k_2 \theta_{,xy} - W^b_{,xy}\right) \\ 0 \end{Bmatrix}; \boldsymbol{\varepsilon}^2 = \begin{Bmatrix} W^s_{,xx} \\ W^s_{,yy} \\ 2W^s_{,xy} \\ 0 \end{Bmatrix}; \tag{17}$$

$$\boldsymbol{\varepsilon}^3 = \begin{Bmatrix} 0 \\ 0 \\ 0 \\ \theta \end{Bmatrix}; \boldsymbol{\gamma}^0 = \begin{Bmatrix} (k_1+1)W^s_{,x} + k_2\theta_{,x} \\ (k_1+1)W^s_{,y} + k_2\theta_{,y} \end{Bmatrix}; \boldsymbol{\gamma}^1 = \begin{Bmatrix} \theta_{,x} \\ \theta_{,y} \end{Bmatrix};$$

$$\boldsymbol{\gamma}^2 = \begin{Bmatrix} W^s_{,x} \\ W^s_{,x} \end{Bmatrix}$$

The linear elastic constitutive relations can be written by:

$$\boldsymbol{\sigma} = \begin{Bmatrix} \sigma_{xx} \\ \sigma_{yy} \\ \sigma_{xy} \\ \sigma_{zz} \\ \sigma_{xz} \\ \sigma_{yz} \end{Bmatrix} = \begin{bmatrix} C_{11} & C_{12} & 0 & C_{13} & 0 & 0 \\ C_{12} & C_{22} & 0 & C_{23} & 0 & 0 \\ 0 & 0 & C_{66} & 0 & 0 & 0 \\ C_{13} & C_{23} & 0 & C_{33} & 0 & 0 \\ 0 & 0 & 0 & 0 & C_{55} & 0 \\ 0 & 0 & 0 & 0 & 0 & C_{44} \end{bmatrix} \begin{Bmatrix} \varepsilon_{xx} \\ \varepsilon_{yy} \\ \varepsilon_{xy} \\ \varepsilon_{zz} \\ \varepsilon_{xz} \\ \varepsilon_{yz} \end{Bmatrix} \tag{18}$$

in which C_{mn} are given by:

$$C_{11} = C_{22} = C_{33} = \frac{(1-\nu(x,z))E(x,z)}{(1-2\nu(x,z))(1+\nu(x,z))};$$
$$C_{12} = C_{13} = C_{23} = \nu(x,z)C_{11};$$

$$C_{66} = C_{55} = C_{44} = \frac{E(x,z)}{(1-2\nu(x,z))(1+\nu(x,z))} \tag{19}$$

2.3. Fluid model

In the present work, the fluid dynamic pressure acting on the plate is expressed as a function of acceleration with the following assumptions (Soni et al. [79]):

1. The fluid flow is homogeneous, incompressible, inviscid and no-rotation motion.
2. The fluid flow is small and hence the amplitude of vibration complies with the small deflection theory.
3. The fluid is assumed to be non-viscous, and hence the fluid pressure impacting on the plate is completely normal to the plate surface.
4. The influence of boundary conditions on the number of a plane wave is neglected.
5. The length of the plate is smaller than the level of fluid below the plate, and hence the rigid bottom of the fluid container does not affect the dynamics of fluid-plate.
6. The plate in-plane dimensions are smaller than the length and width of the container, and hence the walls of the container do not participate in the vibrations of the plate in contact with the fluid.
7. The effect of the non-linearity at the interface of the fluid-plate is neglected.
8. The thickness of the plate is thin, and hence the formulation of in-plane forces can neglect the effect of fluid forces.

The BDFG rectangular plates with the fluid dynamic pressure are modelled for the case of the horizontally submerged plate as shown in Fig. 3, and for the case of the vertically immersed plate as shown in Fig. 4. For both the horizontal and vertical configurations, this section derives a general differential equation governing the velocity potential as

$$\nabla^2\phi = \frac{\partial^2\phi}{\partial x^2} + \frac{\partial^2\phi}{\partial y^2} + \frac{\partial^2\phi}{\partial z^2} = 0 \tag{20}$$

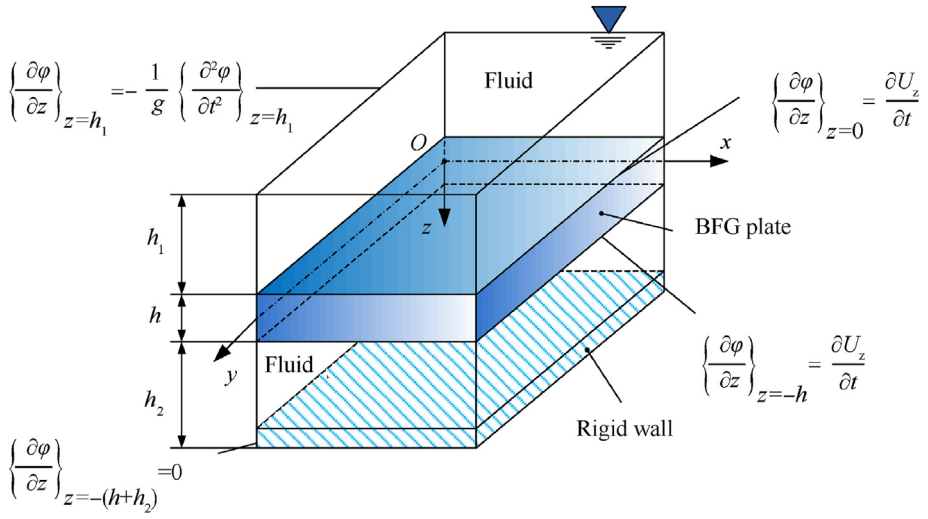

Fig. 3. Plate-fluid model bounded by a rigid wall.

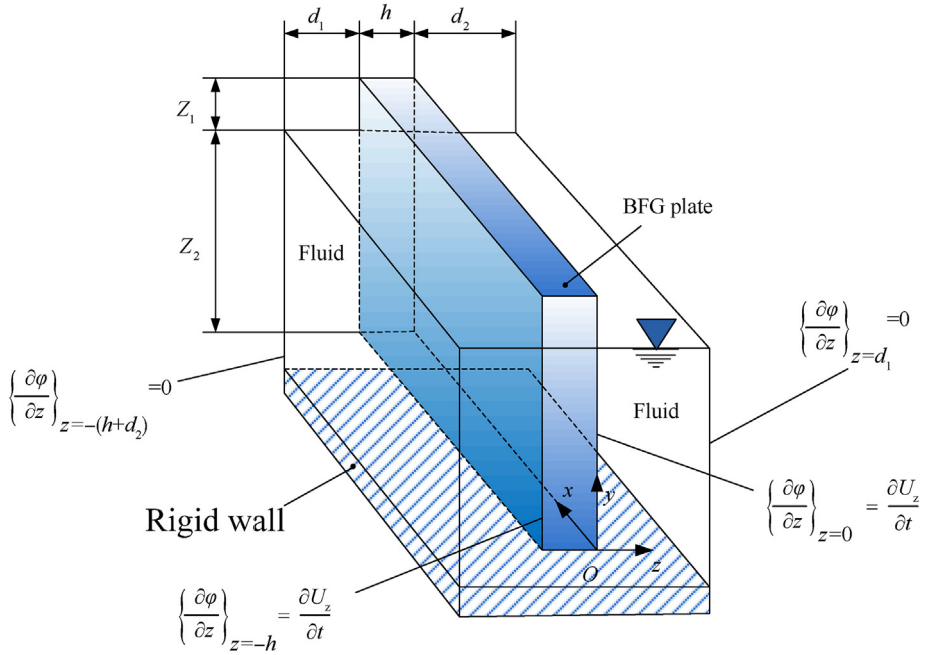

Fig. 4. Vertical plate partially submerged in a fluid tank.

The boundary conditions for the horizontal and vertical plates are then dealt with separately. Using Bernoulli's equation and neglecting its nonlinear terms, the fluid pressure at any point of the fluid-plate interface can be expressed as:

$$P_{\text{upper}} = P_{\text{right}} = P_{z=0} = -\rho_{\text{f}}\left(\frac{\partial \phi}{\partial t}\right)_{z=0} \tag{21}$$

$$P_{\text{lower}} = P_{\text{left}} = P_{z=-h} = -\rho_{\text{f}}\left(\frac{\partial \phi}{\partial t}\right)_{z=-h} \tag{22}$$

where ρ_{f} is the fluid mass density.

The following separate variable relation is assumed for the potential velocity function:

$$\phi(x, y, z, t) = F(z)Q(x, y, t) \tag{23}$$

where $F(z)$ and $Q(x, y, t)$ are two separate functions needing to be determined from fluid boundary conditions. It is assumed that for a permanent contract that exists between the plate surface and peripheral fluid layer, the out-of-plane velocity component of the fluid on the plate surface should match the instantaneous rate of change of the plate displacement in the transverse direction. So at the fluid-plate interfaces, the upper/right plate-fluid interface and lower/left plate-fluid interface, can be expressed, respectively, by the following kinematic boundary conditions

$$\left(\frac{\partial \phi}{\partial t}\right)_{=0} = \frac{\partial U_z}{\partial t} \tag{24}$$

$$\left(\frac{\partial\phi}{\partial t}\right)_{z=-h}=\frac{\partial U_z}{\partial t} \tag{25}$$

Substituting Eq. (23) into Eqs. (24) and (25), one obtains the relationship between two separated functions of the velocity potential as:

$$Q(x,y,t)=\frac{1}{\left(\mathrm{d}F(z)/\mathrm{d}z\right)_{z=0}}\frac{\partial U_z}{\partial t} \tag{26}$$

$$Q(x,y,t)=\frac{1}{\left(\mathrm{d}F(z)/\mathrm{d}z\right)_{z=-h}}\frac{\partial U_z}{\partial t} \tag{27}$$

The velocity potential on fluid-plate interfaces can be expressed by substituting Eqs. (26) and (27) into Eq. (23) as

$$\phi(x,y,z,t)=\frac{F(z)}{\left(\mathrm{d}F(z)/\mathrm{d}z\right)_{z=0}}\frac{\partial U_z}{\partial t} \tag{28}$$

$$\phi(x,y,z,t)=\frac{F(z)}{\left(\mathrm{d}F(z)/\mathrm{d}z\right)_{z=-h}}\frac{\partial U_z}{\partial t} \tag{29}$$

Eq. (20) can now be recast in terms of the lateral deflection of the plate by introducing Eqs. (28) and (29). The resulting second-order general differential equation can be written as

$$\frac{\mathrm{d}^2F(z)}{\mathrm{d}z^2}-\gamma^2F(z)=0 \tag{30}$$

The horizontal plate submerged in the fluid medium, $\gamma=\pi\sqrt{\frac{1}{a^2}+\frac{1}{b^2}}$ (Soni et al. [79]). The case of vertical plate, when partially submerged in fluid medium ($Z_2<b$), $\gamma=\pi\sqrt{\frac{1}{a^2}+\frac{1}{Z_2^2}}$ and completely submerged in fluid medium ($Z_2\geq b$), $\gamma=\pi\sqrt{\frac{1}{a^2}+\frac{1}{b^2}}$. The readers can refer more detail in (Kerboua et al. [80]). The general solution of Eq. (30) is given as

$$F(z)=C_1e^{\gamma z}+C_2e^{-\gamma z} \tag{31}$$

Substituting Eq. (31) into Eqs. (28) and (29), one obtains the expression for the velocity potential function on the fluid-plate interface as follows:

$$\phi(x,y,z,t)=\frac{C_1e^{\gamma z}+C_2e^{-\gamma z}}{\left(\mathrm{d}F(z)/\mathrm{d}z\right)_{z=0}}\frac{\partial U_z}{\partial t} \tag{32}$$

$$\phi(x,y,z,t)=\frac{C_1e^{\gamma z}+C_2e^{-\gamma z}}{\left(\mathrm{d}F(z)/\mathrm{d}z\right)_{z=-h}}\frac{\partial U_z}{\partial t} \tag{33}$$

where C_1, C_2 are the integral constants determined according to contact boundary conditions between the fluid and the plate.

2.3.1. Dynamic pressure for horizontally submerged plate

For the case of the horizontally submerged plate (Fig. 3), the fluid extreme boundary conditions include the free fluid surface at $z=h_1$ and the rigid bottom surface at $z=h+h_2$. Thus, the potential function corresponding to the boundary conditions is determined by:

For the free fluid surface:

$$\left(\frac{\partial\phi}{\partial z}\right)_{z=h_1}=-\frac{1}{g}\left(\frac{\partial^2\phi}{\partial t^2}\right)_{z=h_1} \tag{34}$$

$$\text{For the rigid bottom of the tank}: \left(\frac{\partial\phi}{\partial z}\right)_{z=h+h_2}=0 \tag{35}$$

where g represents the gravity acceleration.

Considering the velocity potential ϕas a function of sinusoidal time dependence:

$$\phi(x,y,z,t)=F(z)Q_1(x,y)e^{-i\omega t} \tag{36}$$

Substituting Eq. (36) into Eq. (34), we obtain

$$\left(\frac{\partial F(z)}{\partial z}\right)_{z=h_1}=\frac{\omega^2}{g}(F(z))_{z=h_1} \tag{37}$$

Substituting Eq. (31) into Eq. (37), we obtain

$$C_2=Xe^{2\gamma h_1}C_1 \tag{38}$$

where $X=\frac{g\gamma-\omega^2}{g\gamma+\omega^2}$ (Kerboua et al. [80]; Haddara and Cao [81]) demonstrated that the value of X tends asymptotically towards -1 using the graphical approach. In the present work, the approximate value of $X=-1$ is used in order to avoid the effect of nonlinearity on the fluid-plate interface.

Similarly, substituting Eq. (32) into Eq. (24), one finds

$$C_1-C_2=\frac{1}{\gamma}\left(\frac{\partial F(z)}{\partial z}\right)_{z=0} \tag{39}$$

From Eqs. (38) and (39), we obtain the results

$$C_1=\frac{1}{\gamma\left(1-Xe^{2\gamma h_1}\right)}\left(\frac{\partial F(z)}{\partial z}\right)_{z=0};\ C_2=\frac{e^{2\gamma h_1}}{\gamma\left(1-Xe^{2\gamma h_1}\right)}\left(\frac{\partial F(z)}{\partial z}\right)_{z=0} \tag{40}$$

Substituting Eq. (40) into Eq. (32), we get the required relation for the potential function of the fluid on the upper portion of the plate as

$$\phi(x,y,z,t)=\frac{e^{\gamma z}+Xe^{-\gamma(z-2h_1)}}{\gamma\left(1-Xe^{2\gamma h_1}\right)}\frac{\partial U_z}{\partial t} \tag{41}$$

Similarly, by substituting Eq. (33) into Eqs. (35) and (25), we get the required relation for the velocity potential function of the fluid in the lower portion of the plate as

$$\phi(x,y,z,t)=\frac{e^{\gamma z}+e^{-\gamma(z+2h+2h_2)}}{\gamma\left(e^{-\gamma h}-e^{-\gamma(h+2h_2)}\right)}\frac{\partial U_z}{\partial t} \tag{42}$$

Substituting Eq. (41) into Eq. (21), the fluid dynamic pressure acting on the upper surface of the plate can be expressed as

$$P_{\text{upper}}=-\frac{\rho_f}{\gamma}\frac{1+Xe^{2\gamma h_1}}{\left(1-Xe^{2\gamma h_1}\right)}\frac{\partial^2U_z}{\partial t^2} \tag{43}$$

Similarly, substituting Eq. (42) into Eq. (22), the fluid dynamic pressure acting on the lower surface of the plate is expressed as

$$P_{\text{lower}}=-\frac{\rho_f}{\gamma}\frac{1+e^{-2\gamma h_2}}{-1+e^{-2\gamma h_2}}\frac{\partial^2U_z}{\partial t^2} \tag{44}$$

Now, the difference of the fluid dynamic pressure between the

upper and lower surfaces ((ΔP) for the horizontally submerged plate can be written as

$$\Delta P = P_{\text{upper}} - P_{\text{lower}} = -\frac{\rho_f}{\gamma}\left(\frac{1+Xe^{2\gamma h_1}}{(1-Xe^{2\gamma h_1})} - \frac{1+e^{-2\gamma h_2}}{-1+e^{-2\gamma h_2}}\right)$$
$$\frac{\partial^2 U_z}{\partial t^2} = m_{\text{add}}\frac{\partial^2 U_z}{\partial t^2} \tag{45}$$

where $m_{\text{add}} = -\frac{\rho_f}{\gamma}\left(\frac{1+Xe^{2\gamma h_1}}{(1-Xe^{2\gamma h_1})} - \frac{1+e^{-2\gamma h_2}}{-1+e^{-2\gamma h_2}}\right)$ is the virtual added mass due to the fluid in the case of a horizontally submerged plate. When a plate vibrates in a fluid medium then its mass is increased by the mass of the virtual layer of vibrating fluid and this phenomenon is called the added virtual mass effect.

2.3.2. Dynamic pressure for vertical submerged plate

For the case of vertical plate partially immersed in fluid as shown in Fig. 4, the difference of the dynamic pressure ΔP of surrounding fluid may be expressed as:

$$\Delta P = P_{\text{right}} - P_{\text{left}} \tag{46}$$

where $P_{\text{right}}, P_{\text{left}}$ are the fluid dynamic pressures acting to the right and left surfaces of the plate. The boundary conditions for the fluid-plate interface on left and right ends are given by:

$$\left(\frac{\partial \phi}{\partial t}\right)_{z=d_1} = 0 \tag{47}$$

$$\left(\frac{\partial \phi}{\partial t}\right)_{z=-h-d_1} = 0 \tag{48}$$

From Eqs. (24), (32) and (47), the expression for velocity potential function on the right side of the plate becomes

$$\phi(x,y,z,t) = \frac{e^{\gamma z} + e^{-\gamma(z-2d_1)}}{\gamma\left(1-e^{2\gamma d_1}\right)}\frac{\partial U_z}{\partial t} \tag{49}$$

Similarly, from Eqs. (25), (33) and (48), the expression for velocity potential function on the left side of the plate becomes

$$\phi(x,y,z,t) = \frac{e^{\gamma z} + e^{-\gamma(z+2h+2d_2)}}{\gamma\left(e^{-\gamma h} - e^{-\gamma(h+2d_2)}\right)}\frac{\partial U_z}{\partial t} \tag{50}$$

From Eqs. ((22), (46), (49) and (50), the total difference of the dynamic fluid pressure ΔP for vertically submerged plate conditions is expressed as

$$\Delta P = P_{\text{right}} - P_{\text{left}} = -\frac{\rho_f}{\gamma}\left(\frac{1+e^{2\gamma d_1}}{(1-e^{2\gamma d_1})} - \frac{1+e^{-2\gamma d_2}}{-1+e^{-2\gamma d_2}}\right)$$
$$\frac{\partial^2 U_z}{\partial t^2} = m_{\text{add}}\frac{\partial^2 U_z}{\partial t^2} \tag{51}$$

where $m_{\text{add}} = -\frac{\rho_f}{\gamma}\left(\frac{1+e^{2\gamma d_1}}{(1-e^{2\gamma d_1})} - \frac{1+e^{-2\gamma d_2}}{-1+e^{-2\gamma d_2}}\right)$ is the virtual added mass due to fluid when the plate is vertical and partially submerged in the fluid medium.

2.4. The governing equation

The equations of motion of the BDFG plate in the fluid medium are based on the refined three-dimensional plate theory derived from Hamilton's principle by:

$$\int_{t_1}^{t_2}(\delta U + \delta W - \delta T)\mathrm{d}t = 0 \tag{52}$$

where δU, δW and δT are the variation of the strain energy, external work and kinetic energy. The variation of the strain energy can be given by:

$$\delta U = \int_S\int_{-\frac{h}{2}}^{+\frac{h}{2}}\sigma_{ij}\delta\varepsilon_{ij}\mathrm{d}z\mathrm{d}x\mathrm{d}y = \int_S\left(\boldsymbol{\varepsilon}^{\mathrm{T}}\boldsymbol{D}_{\mathrm{b}}\delta\boldsymbol{\varepsilon} + \boldsymbol{\gamma}^{\mathrm{T}}\boldsymbol{D}_{\mathrm{s}}\delta\boldsymbol{\gamma}\right)\mathrm{d}x\mathrm{d}y \tag{53}$$

where

$$\boldsymbol{D}_{\mathrm{b}} = \begin{bmatrix} \boldsymbol{A} & \boldsymbol{B} & \boldsymbol{B}^b & \boldsymbol{X} \\ \boldsymbol{B} & \boldsymbol{F} & \boldsymbol{F}^{\mathrm{b}} & \boldsymbol{Y} \\ \boldsymbol{B}^{\mathrm{b}} & \boldsymbol{F}^{\mathrm{b}} & \boldsymbol{H} & \boldsymbol{Y}^{\mathrm{b}} \\ \boldsymbol{X} & \boldsymbol{Y} & \boldsymbol{Y}^{\mathrm{b}} & \boldsymbol{H}^{\mathrm{b}} \end{bmatrix}; \boldsymbol{D}_{\mathrm{s}} = \begin{bmatrix} \boldsymbol{A}_{\mathrm{s}} & \boldsymbol{B}_{\mathrm{s}} & \boldsymbol{B}^{\mathrm{b}}{}_{\mathrm{s}} \\ \boldsymbol{B}_{\mathrm{s}} & \boldsymbol{F}_{\mathrm{s}} & \boldsymbol{F}^{\mathrm{b}}{}_{\mathrm{s}} \\ \boldsymbol{B}^{\mathrm{b}}{}_{\mathrm{s}} & \boldsymbol{F}^{\mathrm{b}}{}_{\mathrm{s}} & \boldsymbol{H}_{\mathrm{s}} \end{bmatrix} \tag{54}$$

$$\left(\boldsymbol{A},\boldsymbol{B},\boldsymbol{B}^{\mathrm{b}},\boldsymbol{F},\boldsymbol{F}^{\mathrm{b}},\boldsymbol{H}\right) = \int_{\frac{-h}{2}}^{\frac{h}{2}}\boldsymbol{Q}_{\mathrm{b}}\left(1,z,f(z),z^2,zf(z),f(z)^2\right)\mathrm{d}z$$

$$\left(\boldsymbol{X},\boldsymbol{Y},\boldsymbol{Y}^{\mathrm{b}},\boldsymbol{H}^{\mathrm{b}}\right) = \int_{\frac{-h}{2}}^{\frac{h}{2}}\boldsymbol{Q}_{\mathrm{b}}\left(g'(z),zg'(z),f(z)g'(z),g'(z)^2\right)\mathrm{d}z$$

$$\left(\boldsymbol{A}_{\mathbf{s}},\boldsymbol{B}_{\mathbf{s}},\boldsymbol{B}^{\mathbf{b}}{}_{\mathbf{s}},\boldsymbol{F}_{\mathbf{s}},\boldsymbol{F}^{\mathrm{b}},\boldsymbol{H}_{\mathbf{s}}\right) = \int_{\frac{-h}{2}}^{\frac{h}{2}}\boldsymbol{Q}_{\mathrm{s}}\left(1,z,f(z),z^2,zf(z),f(z)^2\right)\mathrm{d}z \tag{55}$$

$$\boldsymbol{Q}_{\mathrm{b}} = \begin{bmatrix} C_{11} & C_{12} & 0 & C_{13} \\ C_{12} & C_{22} & 0 & C_{23} \\ 0 & 0 & C_{66} & 0 \\ C_{13} & C_{23} & 0 & C_{33} \end{bmatrix}; \boldsymbol{Q}_{\mathrm{s}} = \begin{bmatrix} C_{55} & 0 \\ 0 & C_{44} \end{bmatrix} \tag{56}$$

The variation of external work can be expressed as:

$$\delta W = -\int_S \Delta P\delta U_z\mathrm{d}x\mathrm{d}y \tag{57}$$

where ΔP is the hydrodynamic pressure of fluid, perpendicular to the plate surface and presented in sections 2.3 and Eq. (57) can be written as

$$\delta W = -\int_S m_{\text{add}}\frac{\partial^2 U_z}{\partial t^2}\delta U_z\mathrm{d}x\mathrm{d}y \tag{58}$$

The variation of kinetic energy is given by:

$$\delta T = \int_S\int_{-h/2}^{+h/2}\rho(z)\left(\dot{U}_x\delta\dot{U}_x + \dot{U}_y\delta\dot{U}_y + \dot{U}_z\delta\dot{U}_z\right)\mathrm{d}z\mathrm{d}S = \int_S\left(\ddot{\boldsymbol{u}}^{\mathrm{T}}\boldsymbol{H}_{\mathrm{m}}\delta\boldsymbol{u}\right)\mathrm{d}x\mathrm{d}y \tag{59}$$

$$\boldsymbol{u}=\left\{\begin{array}{cccccccccccc} U_0 & V_0 & W^{\mathrm{b}} & W^{\mathrm{s}} & \theta & \frac{\partial W^{\mathrm{b}}}{\partial x} & \frac{\partial W^{\mathrm{s}}}{\partial x} & \frac{\partial W^{\mathrm{b}}}{\partial y} & \frac{\partial W^{\mathrm{s}}}{\partial y} & \frac{\partial \theta}{\partial x} & \frac{\partial \theta}{\partial y} \end{array}\right\}^{\mathrm{T}} \tag{60}$$

$$\boldsymbol{H}_{\mathrm{m}}=\int_{-\frac{h}{2}}^{+\frac{h}{2}} \rho(x,z)\boldsymbol{L}_{\mathrm{m}}^{\mathrm{T}}\boldsymbol{L}_{\mathrm{m}}\mathrm{d}z \tag{61}$$

$$\boldsymbol{L}_{\mathrm{m}}=\begin{bmatrix} 1 & 0 & 0 & 0 & 0 & -z & f+zk_1 & 0 & 0 & zk_2 & 0 \\ 0 & 1 & 0 & 1 & 0 & 0 & 0 & -z & f+zk_1 & 0 & zk_2 \\ 0 & 0 & 1 & 1 & g & 0 & 0 & 0 & 0 & 0 & 0 \end{bmatrix} \tag{62}$$

where $\dot{(\ )}$, $\ddot{(\ )}$ are the first and second-order derivatives over time, respectively. Then integrating through the thickness of the plate, the coefficients in Eqs. (55) and (61) are obtained as a function of length variable x.

Substituting Eqs. (53), (57) and (59) into Eq. (52), a weak form of the plate in fluid medium can be described as:

$$\int_S\left(\boldsymbol{\varepsilon}^{\mathrm{T}}\boldsymbol{D}_{\mathrm{b}}\delta\boldsymbol{\varepsilon}+\boldsymbol{\gamma}^{\mathrm{T}}\boldsymbol{D}_{\mathrm{s}}\delta\gamma\right)\mathrm{d}x\mathrm{d}y=\int_S m_{\mathrm{add}}\frac{\partial^2 U_z}{\partial t^2}\delta U_z\mathrm{d}x\mathrm{d}y + \int_S(\ddot{\boldsymbol{u}}^{\mathrm{T}}\boldsymbol{H}_{\mathrm{m}}\delta\boldsymbol{u})\mathrm{d}x\mathrm{d}y \tag{63}$$

3. NURBS − based IGA for free vibration analysis of plates in the fluid medium

3.1. NURBS basis functions

In the IGA, the knot vector $\boldsymbol{k}(\zeta)$is defined as the nondecreasing numbers between zero and one $\boldsymbol{k}(\zeta)=\{\zeta_1=0,\ldots,\zeta_i,\ldots,\zeta_{n+p+1}=1\}$, where i represents the knot index; $\zeta_i$is called the i^{th} knot; n is the number of basic functions, and p is the order of the polynomial. The univariate B − spline basis function $N_{i,p}(\zeta)$, is defined recursively by (Hughes et al. [38]):

$$N_{i,p}(\zeta)=\begin{cases} 1 & \text{if } \zeta_i\le\zeta\le\zeta_{i+1} \\ 0 & \text{otherwise} \end{cases} \quad \text{for } p=0 \tag{64}$$

and

$$N_{i,p}(\zeta)=\frac{\zeta-\zeta_i}{\zeta_{i+p}-\zeta_i}N_{i,p-1}(\zeta)+\frac{\zeta_{i+p+1}-\zeta}{\zeta_{i+p+1}-\zeta_{i+1}}N_{i+1,p-1}(\zeta) \text{ for } p\ge 1 \tag{65}$$

Two-dimensional NURBS basis functions can be constructed by taking the tensor product of the univariate B − spline basis functions in two parametric dimensions ζ and η

$$R_{i,j}^{p,q}(\zeta,\eta)=\frac{N_{i,p}(\zeta)N_{j,q}(\eta)w_{i,j}}{\sum_{i=1}^{n}\sum_{j=1}^{m}N_{i,p}(\zeta)N_{j,q}(\eta)w_{i,j}} \tag{66}$$

where $w_{i,j}$are the weight; $N_{i,p}(\zeta)$ and $N_{j,q}(\eta)$ represent the B − spline basis functions of order p in the ζ and order q in the η direction, respectively; $N_{j,q}(\eta)$ follows the recursive formula shown in Eq. (65) with knot vector $\boldsymbol{k}(\eta)$, which is defined in the same manner as $\boldsymbol{k}(\zeta)$.

3.2. NURBS based formulation

The displacements in the middle plane of the plate are approximated as follows:

$$\boldsymbol{q}^h=\sum_{I=1}^{NN}R_I\boldsymbol{q}_I \tag{67}$$

with

$$\boldsymbol{q}_{\boldsymbol{I}}=\left[U_{0I},V_{0I},W_I^{\mathrm{b}},W_I^{\mathrm{s}},\theta_I\right] \tag{68}$$

where $NN=(p+1)(q+1)$ is the number of control points per physical element; R_I and $\boldsymbol{q}_I$ denote the shape function and the unknown displacement vector at control point I, respectively.

The displacements $U_0,V_0,W^{\mathrm{b}},W^{\mathrm{s}},\theta$ are written in matrices as follows:

$$U_0=\sum_{I=1}^{NN}[R_I\quad 0\quad 0\quad 0\quad 0]\boldsymbol{q}_I=\sum_{I=1}^{NN}\boldsymbol{N}_{uI}\boldsymbol{q}_I \tag{69}$$

$$V_0=\sum_{I=1}^{NN}[0\quad R_I\quad 0\quad 0\quad 0]\boldsymbol{q}_I=\sum_{I=1}^{NN}\boldsymbol{N}_{vI}\boldsymbol{q}_I \tag{70}$$

$$W^{\mathrm{b}}=\sum_{I=1}^{NN}[0\quad 0\quad R_I\quad 0\quad 0]\boldsymbol{q}_I=\sum_{I=1}^{NN}\boldsymbol{N}_{wbI}\boldsymbol{q}_I \tag{71}$$

$$W^{\mathrm{s}}=\sum_{I=1}^{NN}[0\quad 0\quad 0\quad R_I\quad 0]\boldsymbol{q}_I=\sum_{I=1}^{NN}\boldsymbol{N}_{wsI}\boldsymbol{q}_I \tag{72}$$

$$\theta=\sum_{I=1}^{NN}[0\quad 0\quad 0\quad 0\quad R_I]\boldsymbol{q}_I=\sum_{I=1}^{NN}\boldsymbol{N}_{\theta I}\boldsymbol{q}_I \tag{73}$$

Substituting Eqs. (69)–(73) into Eq. (17), the in-plane, shear and normal strains can be rewritten as

$$\boldsymbol{\varepsilon}^0=\sum_{I=1}^{NN}\boldsymbol{B}_I^0\boldsymbol{q}_I;\boldsymbol{\varepsilon}^1=\sum_{I=1}^{NN}\boldsymbol{B}_I^1\boldsymbol{q}_I;\boldsymbol{\varepsilon}^2=\sum_{I=1}^{NN}\boldsymbol{B}_I^2\boldsymbol{q}_I;\boldsymbol{\varepsilon}^3=\sum_{I=1}^{NN}\boldsymbol{B}_I^3\boldsymbol{q}_I;$$

$$\gamma^0=\sum_{I=1}^{NN}\boldsymbol{B}_I^{s0}\boldsymbol{q}_I;\gamma^1=\sum_{I=1}^{NN}\boldsymbol{B}_I^{s1}\boldsymbol{q}_I;\gamma^2=\sum_{I=1}^{NN}\boldsymbol{B}_I^{s2}\boldsymbol{q}_I \tag{74}$$

in which

$$\boldsymbol{B}_I^0=\begin{bmatrix}\boldsymbol{N}_{uI,x}\\ \boldsymbol{N}_{vI,y}\\ \boldsymbol{N}_{uI,y}+\boldsymbol{N}_{vI,x}\\ 0\end{bmatrix};\boldsymbol{B}_I^1=\begin{bmatrix}k_1\boldsymbol{N}_{wsI,xx}+k_2\boldsymbol{N}_{\theta I,xx}-\boldsymbol{N}_{wbI,xx}\\ k_1\boldsymbol{N}_{wsI,yy}+k_2\boldsymbol{N}_{\theta I,yy}-\boldsymbol{N}_{wbI,yy}\\ 2\left(k_1\boldsymbol{N}_{wsI,xy}+k_2\boldsymbol{N}_{\theta I,xy}-\boldsymbol{N}_{wbI,xy}\right)\\ 0\end{bmatrix};$$

$$\boldsymbol{B}_I^2=\begin{bmatrix}\boldsymbol{N}_{wsI,xx}\\ \boldsymbol{N}_{wsI,yy}\\ 2\boldsymbol{N}_{wsI,xy}\\ 0\end{bmatrix};\boldsymbol{B}_I^{s0}=\begin{bmatrix}(k_1+1)\boldsymbol{N}_{wsI,x}+k_2\boldsymbol{N}_{\theta I,x}\\ (k_1+1)\boldsymbol{N}_{wsI,y}+k_2\boldsymbol{N}_{\theta I,y}\end{bmatrix};$$

$$\boldsymbol{B}_I^{s1}=\begin{bmatrix}\boldsymbol{N}_{\theta I,x}\\ \boldsymbol{N}_{\theta I,y}\end{bmatrix};\boldsymbol{B}_I^{s2}=\begin{bmatrix}\boldsymbol{N}_{wsI,x}\\ \boldsymbol{N}_{wsI,y}\end{bmatrix};\boldsymbol{B}_I^3=\begin{bmatrix}0\\ 0\\ 0\\ \boldsymbol{N}_{\theta I}\end{bmatrix} \tag{75}$$

Substituting Eqs. (69)–(73) into Eq. (60), the displacement field $\boldsymbol{u}$ is obtained as:

$$\boldsymbol{u}=\sum_{I=1}^{NN}\boldsymbol{N}_{mI}\boldsymbol{q}_I \tag{76}$$

where

$$\boldsymbol{N}_{mI}=\left[\boldsymbol{N}_u\ \boldsymbol{N}_v\ \boldsymbol{N}_{wb}\ \boldsymbol{N}_{ws}\ \boldsymbol{N}_\theta\ \boldsymbol{N}_{wb,x}\ \boldsymbol{N}_{ws,x}\ \boldsymbol{N}_{wb,y}\ \boldsymbol{N}_{ws,y}\ \boldsymbol{N}_{\theta,x}\ \boldsymbol{N}_{\theta,y}\right]^{\mathrm{T}}; \tag{77}$$

The displacement $U_z$is written by

$$U_z=\sum_{I=1}^{NN}[0\quad 0\quad R_I\quad R_I\quad 0]\boldsymbol{q}_I=\sum_{I=1}^{NN}\boldsymbol{B}_{wI}\boldsymbol{q}_I \tag{78}$$

Substituting Eqs. (76)–(78) into Eq. (63), the matrix form of the global equilibrium equations for the free vibration analysis of the BDFG plates in the fluid medium is determined by

$$\left(\mathbb{K}-\omega^2\mathbb{M}\right)q=0 \tag{79}$$

in which the stiffness matrix $\mathbb{K}=\sum_{I=1}^{NN}\mathbb{K}_I$ is calculated by

$$\mathbb{K}_I=\mathbb{K}^b+\mathbb{K}^s \tag{80}$$

where

$$\mathbb{K}^{\mathrm{b}}=\int_{\mathrm{S}}\begin{Bmatrix}\boldsymbol{B}^0\\ \boldsymbol{B}^1\\ \boldsymbol{B}^2\\ \boldsymbol{B}^3\end{Bmatrix}^{\mathrm{T}}\begin{bmatrix}\boldsymbol{A} & \boldsymbol{B} & \boldsymbol{B}^{\mathrm{b}} & \boldsymbol{X}\\ \boldsymbol{B} & \boldsymbol{F} & \boldsymbol{F}^{\mathrm{b}} & \boldsymbol{Y}\\ \boldsymbol{B}^{\mathrm{b}} & \boldsymbol{F}^{\mathrm{b}} & \boldsymbol{H} & \boldsymbol{Y}^{\mathrm{b}}\\ \boldsymbol{X} & \boldsymbol{Y} & \boldsymbol{Y}^{\mathrm{b}} & \boldsymbol{H}^{\mathrm{b}}\end{bmatrix}\begin{Bmatrix}\boldsymbol{B}^0\\ \boldsymbol{B}^1\\ \boldsymbol{B}^2\\ \boldsymbol{B}^3\end{Bmatrix}\mathrm{d}x\mathrm{d}y \tag{81}$$

$$\mathbb{K}^s=\int_{\mathrm{S}}\begin{Bmatrix}\boldsymbol{B}^{s0}\\ \boldsymbol{B}^{s1}\\ \boldsymbol{B}^{s2}\end{Bmatrix}^{\mathrm{T}}\begin{bmatrix}\boldsymbol{A}_{\mathrm{s}} & \boldsymbol{B}_{\mathrm{s}} & \boldsymbol{B}^{\mathrm{b}}{}_{\mathrm{s}}\\ \boldsymbol{B}_{\mathrm{s}} & \boldsymbol{F}_{\mathrm{s}} & \boldsymbol{F}^{\mathrm{b}}{}_{\mathrm{s}}\\ \boldsymbol{B}^{\mathrm{b}}{}_{\mathrm{s}} & \boldsymbol{F}^{\mathrm{b}}{}_{\mathrm{s}} & \boldsymbol{H}_{\mathrm{s}}\end{bmatrix}\begin{Bmatrix}\boldsymbol{B}^{s0}\\ \boldsymbol{B}^{s1}\\ \boldsymbol{B}^{s2}\end{Bmatrix}\mathrm{d}x\mathrm{d}y \tag{82}$$

and the mass matrix $\mathbb{M}=\sum_{I=1}^{NN}\mathbb{M}_I$ is computed by

$$\mathbb{M}_I=\mathbb{M}^p+\mathbb{M}^l \tag{83}$$

where $\mathbb{M}^p$, $\mathbb{M}^l$are the mass matrix of the plate and the mass matrix of fluid-plate:

Table 1
Mechanical properties of the BDFG plate ([26,82]).

Materials	E/GPa	ν	ρ/(kg/m^{-3})	Materials	E/GPa	ν	ρ/(kg/m^{-3})
Al	70	0.3	2700	SUS_3O_4	201.04	0.24	2370
Al_2O_3	380	0.3	3800	Si_3N_4	348.43	0.3	8166

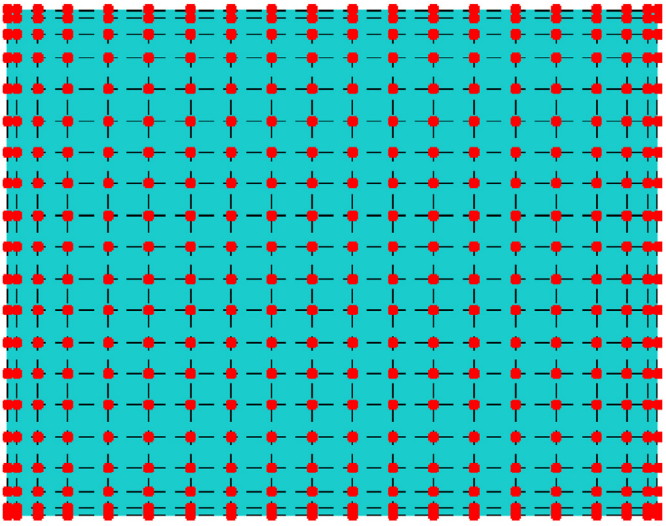

Fig. 5. The mesh of 20 × 20 control points for a square plate.

Table 2
Comparison of dimensionless frequency $\overline{\Omega}_1$of the Al/Al_2O_3 rectangular plate with the SSSS boundary condition.

a/h	Method	p_z			
		Control points	0	1	10
5	Present	12 × 12	5.3119	4.1670	3.3102
		20 × 20	5.3128	4.1676	3.3104
	Quasi 3D-IGA [82]	14 × 14	5.3090	4.1521	3.3126
	RPT-IGA [82]	14 × 14	5.2813	4.0781	3.2519
	TSDT-Navier's [83]		5.2813	4.0781	3.2514
20	Present	12 × 12	5.9302	4.6050	3.8153
		20 × 20	5.9304	4.6048	3.8153
	Quasi 3D-IGA [82]	14 × 14	5.9235	4.5919	3.8129
	RPT-IGA [82]	14 × 14	5.9199	4.5228	3.7623
	TSDT-Navier's [83]		5.9199	4.5228	3.7622
100	Present	12 × 12	5.9797	4.6397	3.8588
		20 × 20	5.9798	4.6397	3.8588
	Quasi 3D-IGA [82]	14 × 14	5.9723	4.6263	3.8533
	RPT-IGA [82]	14 × 14	5.9712	4.5579	3.8058
	TSDT-Navier's [83]		5.9712	4.5579	3.8058

$$\mathbb{M}^p=\int_{\mathrm{S}}(\boldsymbol{N}_{\mathrm{m}})^{\mathrm{T}}\boldsymbol{H}_{\mathrm{m}}\boldsymbol{N}_{\mathrm{m}}\mathrm{d}x\mathrm{d}y \tag{84}$$

$$\mathbb{M}^l=m_{\mathrm{add}}\int_{\mathrm{S}}(\boldsymbol{B}_{\mathrm{w}})^{\mathrm{T}}\boldsymbol{B}_{\mathrm{w}}\mathrm{d}x\mathrm{d}y \tag{85}$$

in which, ω is the natural frequency value.

4. Numerical examples

In this section, some numerical results are performed by using

Table 3
Comparison of the natural frequencies ω(Hz) of the horizontally FG plate (with the SFSF boundary condition) in a vacuum and submerged in fluid.

Mode no.	In vacuum		Plate horizontally submerged in fluid	
	Present	MPT [84]	Present	FEM [80]
1	51.066	51.005	31.229	31.28
2	205.923	205.530	125.945	126.40
3	230.988	228.131	141.613	141.78
4	466.124	464.979	285.158	285.98
5	495.677	490.227	303.938	304.57

Matlab's codes based on the proposed theoretical formulation for BDFG plates submerged in the fluid medium. The $(p+1)(q+1)$Gaussian quadrature is adopted for two-dimensional elements, where p and q represent the orders of the NURBS basis function along the $\zeta$and η directions in the parametric domain, respectively (Hughes et al. [38]). In order to demonstrate the accuracy of the present IGA models, the comparative analyses of vibration are given as

$$\overline{\Omega}_{\mathrm{m}}=\omega_{\mathrm{m}}\frac{a^2}{h}\sqrt{\frac{\rho_{\mathrm{c}}}{E_{\mathrm{c}}}};\Omega_{\mathrm{m}}=\omega_{\mathrm{m}}\frac{a^2}{\pi^2}\sqrt{\frac{\rho_{\mathrm{c}}h}{D_{\mathrm{c}}}};\beta_{\mathrm{m}}=\omega_{\mathrm{m}}a^2\sqrt{\frac{\rho_{\mathrm{c}}h}{D_{\mathrm{c}}}};D_{\mathrm{c}}=\frac{E_{\mathrm{c}}h^3}{12\left(1-\nu^2\right)}$$

in which m is the m-th natural frequency; and the material properties of BDFG plate are given in Table 1.

The obtained numerical results of the present work are compared with the following approaches:

- Quasi 3D − IGA: The higher-order Quasi 3D and isogeometric analysis (Nguyen et al. [82]).
- RPT − IGA: Refine higher-order shear deformation plate theory and isogeometric analysis (Nguyen et al. [82]).
- TSDT-Navier's: Third-order shear deformation plate theory and Navier's method (Thai and Kim [83]).
- MPT: Mindlin's plate theory and exact-closed form characteristics equation (Hosseini-Hashemi et al. [84]).
- FEM: Classical plate theory and finite element method (Kerboua et al. [80]).
- FSDT-IGA: First-order shear deformation plate theory and isogeometric analysis (Li et al. [26]).
- Present: refined quasi 3D plate theory and isogeometric analysis.

4.1. Validation study

In order to validate the present theoretical formulation, we compare the obtained results with those of the published works. We first consider the FG plate using Al/Al_2O_3 material with the SSSS boundary condition; the thickness of plate changes from $a/h=5$ to $a/h=100$; the variation of FG material through-thickness of the plate has complied with the Voigt model with the power-law index $p_z=0,\ 1,\ 10$. The FG plates are modelled with 12×12 and 20×20 control points, in which the mesh of 20×20 control points is plotted in Fig. 5. The dimensionless frequency results $\overline{\Omega}_1$ of the present method by the mesh of 20×20 control points are presented in Table 2 and compared to the numerical results of published work in Refs. (Nguyen et al. [82]; Thai and Kim [83]). It is seen that the obtained results illustrated convincingly the computational convergence and precision of the current IGA model.

Next, let us consider the FG plates horizontal submerged in the fluid medium. The dimensional parameters and material properties of FG plates include Young's modulus $E=207$ GPa, material density $\rho=7850\ \mathrm{kg/m^3}$, Poisson's ratio $=0.3$, $a=0.655$, $b=0.20165$ and thickness $h=9.36$ mm. The fluid density is taken by 1000 $\mathrm{kg/m^3}$. The plate is horizontally submerged in a rectangular reservoir tank with dimensions of 1.3 m × 0.55 m × 0.8 m. Table 3 presents the natural frequencies of two opposite sides of the FG plates (with the SFSF boundary condition) in a vacuum and horizontally submerged in fluid. It is seen that the obtained numerical results by the proposed method agree well with the results of the exact solution obtained by Mindlin's plate theory (Hosseini-Hashemi et al. [84]) in the vacuum and by the finite element method (Kerboua et al. [80]) when completely submerged in fluid.

Table 4 presents the numerical results of the first two frequencies of FG plates horizontally submerged in a fluid with different fluid levels of the present method compared with the exact solution (Hosseini-Hashemi et al. [84]). It can be found that the obtained results of the present method agree well with those obtained by published work (Hosseini-Hashemi et al. [84]). In particular, in view of Table 4, it is observed to gain the expected results for all boundary conditions: the increase of submerged fluid levels leads to the decrease of frequencies of FG plates. It is also noted that the frequencies of FG plates only decrease slightly when

Table 5
Comparison of the first non-dimensional frequency Ω_1 of the Si_3N_4/SUS_3O_4square BDFG plates with the SSSS and CCCC boundary conditions ($a=1$, $h/a=0.1$, $p_z=1$).

BC	Theory	$p_x=0$	$p_x=2$	$p_x=5$
SSSS	FSDT-IGA [26]	1.1066	0.8604	0.8082
	Present	1.1371	0.8726	0.8179
CCCC	FSDT-IGA [26]	1.9720	1.5170	1.4256
	Present	1.9851	1.5190	1.4291

Table 4
Comparison of the first two frequencies of the plate horizontally submerged in a fluid with various fluid levels.

BC	Mode	Theory	In vacuum	Plate horizontally submerged in a fluid with various fluid levels				
				$h_1/a=0$	0.1	0.3	0.5	2
SSSS	1	MPT [84]	48.3006	41.4293	38.4638	36.9582	36.8523	36.8455
		Present	48.3753	41.4296	38.4813	36.9829	36.8776	36.6373
	2	MPT [84]	76.3360	64.5257	59.9367	57.1981	56.9347	56.9111
		Present	76.4678	65.5536	60.9194	58.5615	58.3957	58.0174
CSCS	1	MPT [84]	88.6635	79.6484	74.4777	72.9584	72.9222	72.9214
		Present	90.3925	78.5004	72.9172	70.0794	69.8799	69.4247
	2	MPT [84]	106.9478	93.4901	87.1999	84.2839	84.1148	84.1058
		Present	109.7650	94.3950	87.7253	84.3314	84.0928	83.5482
SCSS	1	MPT [84]	66.3511	58.3467	54.3177	52.7481	52.6826	52.6801
		Present	66.9685	58.0735	53.9450	51.8464	51.6989	51.3623
	2	MPT [84]	89.7039	77.0089	71.6786	68.8209	68.6026	68.5873
		Present	90.6334	77.9443	72.4380	69.6360	69.4390	68.9894

Table 6
The non-dimensional frequency Ω_1 of the Al/Al_2O_3 square BDFG plates (with the SSSS boundary condition) horizontally submerged in the water.

a/h	p_x	p_z	In vacuum	Horizontally submerged in water (h_1/a)				
				0	0.3	0.5	1	2
5	0	0	1.7785	1.5781	1.4495	1.4358	1.4329	1.4329
		0.5	1.3424	1.1775	1.0746	1.0637	1.0614	1.0614
		1	1.2355	1.0766	0.9788	0.9686	0.9664	0.9664
		2	1.1585	1.0020	0.9074	0.8975	0.8955	0.8954
		10	1.0391	0.8881	0.7992	0.7901	0.7881	0.7881
	1	0	1.2014	1.0448	0.9489	0.9389	0.9368	0.9368
		0.5	1.0752	0.9297	0.8417	0.8325	0.8306	0.8306
		1	1.0374	0.8938	0.8077	0.7988	0.7969	0.7969
		2	1.0092	0.8661	0.7811	0.7723	0.7704	0.7704
		10	0.9602	0.8190	0.7363	0.7278	0.7260	0.7260
	10	0	0.9598	0.8177	0.7346	0.7261	0.7243	0.7242
		0.5	0.9367	0.7979	0.7167	0.7084	0.7066	0.7066
		1	0.9291	0.7913	0.7108	0.7026	0.7008	0.7008
		2	0.9232	0.7861	0.7061	0.6979	0.6961	0.6961
		10	0.9139	0.7780	0.6986	0.6905	0.6888	0.6887
10	0	0	1.9370	1.5431	1.3443	1.3248	1.3207	1.3207
		0.5	1.4549	1.1369	0.9826	0.9677	0.9646	0.9645
		1	1.3449	1.0396	0.8947	0.8808	0.8779	0.8778
		2	1.2725	0.9720	0.8328	0.8195	0.8167	0.8167
		10	1.1512	0.8625	0.7338	0.7216	0.7191	0.7191
	1	0	1.3089	1.0085	0.8669	0.8533	0.8505	0.8504
		0.5	1.1679	0.8909	0.7629	0.7507	0.7481	0.7481
		1	1.1291	0.8563	0.7317	0.7199	0.7174	0.7174
		2	1.1032	0.8315	0.7088	0.6973	0.6948	0.6948
		10	1.0533	0.7860	0.6678	0.6566	0.6543	0.6543
	10	0	1.0464	0.7789	0.6612	0.6501	0.6478	0.6478
		0.5	1.0197	0.7588	0.6440	0.6332	0.6309	0.6309
		1	1.0117	0.7526	0.6387	0.6280	0.6258	0.6257
		2	1.0059	0.7481	0.6348	0.6242	0.6220	0.6220
		10	0.9964	0.7407	0.6285	0.6179	0.6157	0.6157
100	0	0	2.0021	0.7610	0.5762	0.5617	0.5587	0.5587
		0.5	1.5010	0.5461	0.4123	0.4018	0.3997	0.3996
		1	1.3905	0.4940	0.3723	0.3628	0.3609	0.3609
		2	1.3211	0.4575	0.3443	0.3355	0.3337	0.3337
		10	1.1995	0.3990	0.2996	0.2919	0.2903	0.2903
	1	0	1.3531	0.4773	0.3596	0.3504	0.3486	0.3485
		0.5	1.2058	0.4164	0.3133	0.3053	0.3036	0.3036
		1	1.1669	0.3980	0.2993	0.2916	0.2900	0.2900
		2	1.1424	0.3846	0.2890	0.2816	0.2800	0.2800
		10	1.0923	0.3604	0.2705	0.2635	0.2621	0.2621
	10	0	1.0822	0.3552	0.2665	0.2597	0.2582	0.2582
		0.5	1.0539	0.3457	0.2593	0.2527	0.2513	0.2513
		1	1.0456	0.3428	0.2572	0.2506	0.2492	0.2492
		2	1.0400	0.3408	0.2557	0.2491	0.2477	0.2477
		10	1.0304	0.3374	0.2531	0.2466	0.2452	0.2452

the plate is submerged in a fluid with the level. $h_1/a \geq 0.3$.

Lastly, we consider the cases of the Si_3N_4/SUS_3O_4 square BDFG plates with the simply supported and full clamped boundary conditions and with material parameters given in Table 1. Table 5 presents the numerical results of the first dimensionless natural frequencies of BDFG plates of the present method compared to those of published work (Li et al. [26]). It is seen that there is a good agreement between the results obtained by the proposed method and those by the IGA of Li et al. [26]. However, the results by the IGA of Li et al. [26] are slightly smaller than those by the proposed method. It is because the IGA of Li et al. [26] only used the FSDT theory, while the IGA in the present work uses the refined quasi 3D plate theory. The above-compared examples hence verified the accuracy and reliability of the proposed approach.

4.2. Numerical results and discussion

In this section, the influences of different geometric and material parameters (such as the length-to-thickness ratio, width-to-length ratio, power-law indexes), different models of plate submerged in fluid, and different boundary conditions on the natural frequencies of BDFG plates are conducted. The square plate has the geometric parameter $a = 1$ m, and the dimension of tank $5 \times 5 \times 5$ m. The numerical results are presented in tubular and figure forms.

Table 7
The non-dimensional frequency Ω_1 of the Al/Al_2O_3 square BDFG plate (with the SSSS boundary condition) vertically immersed in the water ($d_1 = d_2$).

a/h	p_x	p_z	In vacuum	Vertically immersed in water (Z_2/b)				
				0.1	0.3	0.5	0.7	1
5	0	0	1.7785	1.7146	1.6105	1.5354	1.4829	1.4329
		0.5	1.3424	1.2892	1.2038	1.1431	1.1012	1.0614
		1	1.2355	1.1838	1.1017	1.0438	1.0039	0.9664
		2	1.1585	1.1072	1.0265	0.9701	0.9316	0.8954
		10	1.0391	0.9891	0.9114	0.8580	0.8218	0.7881
	1	0	1.2014	1.1504	1.0695	1.0126	0.9736	0.9368
		0.5	1.0752	1.0276	0.9525	0.9000	0.8642	0.8306
		1	1.0374	0.9902	0.9162	0.8647	0.8297	0.7969
		2	1.0092	0.9620	0.8883	0.8373	0.8027	0.7704
		10	0.9602	0.9133	0.8408	0.7910	0.7573	0.7260
	10	0	0.9598	0.9125	0.8395	0.7895	0.7557	0.7242
		0.5	0.9367	0.8905	0.8192	0.7703	0.7373	0.7066
		1	0.9291	0.8833	0.8125	0.7640	0.7312	0.7008
		2	0.9232	0.8776	0.8072	0.7590	0.7264	0.6961
		10	0.9139	0.8687	0.7988	0.7510	0.7187	0.6887
10	0	0	1.9370	1.7969	1.5988	1.4735	1.3930	1.3207
		0.5	1.4549	1.3396	1.1808	1.0824	1.0201	0.9645
		1	1.3449	1.2331	1.0812	0.9883	0.9297	0.8778
		2	1.2725	1.1612	1.0123	0.9225	0.8663	0.8167
		10	1.1512	1.0423	0.9003	0.8164	0.7645	0.7191
	1	0	1.3089	1.1986	1.0493	0.9583	0.9011	0.8504
		0.5	1.1679	1.0652	0.9280	0.8453	0.7936	0.7481
		1	1.1291	1.0274	0.8926	0.8119	0.7616	0.7174
		2	1.1032	1.0013	0.8673	0.7876	0.7382	0.6948
		10	1.0533	0.9521	0.8208	0.7436	0.6959	0.6543
	10	0	1.0464	0.9449	0.8137	0.7367	0.6892	0.6478
		0.5	1.0197	0.9206	0.7926	0.7175	0.6713	0.6309
		1	1.0117	0.9133	0.7862	0.7117	0.6658	0.6257
		2	1.0059	0.9080	0.7816	0.7074	0.6618	0.6220
		10	0.9964	0.8992	0.7738	0.7004	0.6552	0.6157
100	0	0	2.0021	1.2261	0.8304	0.6871	0.6148	0.5587
		0.5	1.5010	0.8900	0.5968	0.4925	0.4401	0.3996
		1	1.3905	0.8098	0.5401	0.4451	0.3976	0.3609
		2	1.3211	0.7546	0.5007	0.4120	0.3678	0.3337
		10	1.1995	0.6642	0.4371	0.3590	0.3202	0.2903
	1	0	1.3531	0.7838	0.5220	0.4300	0.3841	0.3485
		0.5	1.2058	0.6872	0.4556	0.3749	0.3347	0.3036
		1	1.1669	0.6588	0.4357	0.3583	0.3197	0.2900
		2	1.1424	0.6385	0.4212	0.3461	0.3088	0.2800
		10	1.0923	0.6010	0.3949	0.3242	0.2891	0.2621
	10	0	1.0822	0.5930	0.3892	0.3195	0.2849	0.2582
		0.5	1.0539	0.5771	0.3788	0.3109	0.2772	0.2513
		1	1.0456	0.5724	0.3756	0.3083	0.2749	0.2492
		2	1.0400	0.5691	0.3734	0.3065	0.2733	0.2477
		10	1.0304	0.5635	0.3697	0.3034	0.2705	0.2452

Table 6 displayed the effects of the length-to-thickness ratio a/h, the power-law index p_x, p_z and the fluid depth level h_1/a on the natural frequency Ω_1 of the Al/Al_2O_3 square BDFG plates (with the SSSS boundary condition) horizontally submerged in fluid. It can be seen that the increase of the thickness and the length ratio h_1/a makes the natural frequencies of plate Ω_1 decrease fastly. However, when $h_1/a \geq 1$ these natural frequencies do not change. This can be explained that when $h_1 \geq a$, the virtual added mass $m_{add} \to 2\frac{\rho_f}{\gamma}$(constant) and hence the natural frequency of the plate Ω_1 tends to constant and does not change. In addition, the natural frequency Ω_1 decreases significantly when the power-law indexes p_x, p_z increase. It is noted that when the length-to-thickness ratio

Table 8
The first five non-dimensional frequencies $\Omega_m$of Al/Al_2O_3square BDFG plate horizontally submerged in the water ($a = 1$; $h/a = 0.2$, $p_x = 1$, $p_z = 1$).

BC	Mode	In vacuum	Horizontally submerged in water (h_1/a)				
			0	0.3	0.5	1	2
CCCC	1	2.0019	1.4279	1.2876	1.2731	1.2700	1.2700
	2	3.5995	2.5553	2.3078	2.2821	2.2766	2.2766
	3	3.6052	2.5843	2.3351	2.3091	2.3037	2.3036
	4	4.7189	3.4892	3.1539	3.1189	3.1115	3.1114
	5	4.7568	3.8710	3.4993	3.4602	3.4520	3.4519
CCCS	1	1.8297	1.3139	1.1856	1.1723	1.1695	1.1694
	2	3.2440	2.3292	2.1075	2.0843	2.0794	2.0794
	3	3.5230	2.5356	2.2918	2.2664	2.2610	2.2610
	4	4.1884	3.3483	3.0300	2.9967	2.9896	2.9895
	5	4.6270	3.6674	3.3232	3.2867	3.2790	3.2789
CSCS	1	1.7050	1.2222	1.1031	1.0907	1.0881	1.0881
	2	2.9258	2.1410	1.9408	1.9199	1.9155	1.9154
	3	3.4726	2.4640	2.2264	2.2017	2.1964	2.1964
	4	3.7028	3.2456	2.9405	2.9085	2.9018	2.9017
	5	4.4600	3.4277	3.1642	3.1314	3.1245	3.1244
CFCF	1	1.3009	0.9347	0.8415	0.8319	0.8299	0.8298
	2	1.5782	1.1469	1.0345	1.0228	1.0203	1.0203
	3	2.2089	1.8045	1.6357	1.6180	1.6143	1.6142
	4	2.4608	1.8262	1.8260	1.8260	1.8260	1.8260
	5	3.1082	2.2328	2.0158	1.9932	1.9885	1.9884
CSSS	1	1.4453	1.0426	0.9418	0.9314	0.9291	0.9291
	2	2.8007	2.0511	1.8603	1.8403	1.8361	1.8360
	3	3.0701	2.2095	2.0006	1.9788	1.9742	1.9741
	4	3.6722	3.0579	2.7748	2.7450	2.7387	2.7386
	5	4.0557	3.4002	3.1278	3.0954	3.0885	3.0884
SFSS	1	0.7594	0.5773	0.5221	0.5164	0.5151	0.5151
	2	1.6694	1.2231	1.1085	1.0965	1.0940	1.0940
	3	2.3161	1.7946	1.6300	1.6127	1.6091	1.6091
	4	2.6122	2.3091	2.1128	2.0905	2.0858	2.0857
	5	3.1025	2.3252	2.1729	2.1510	2.1463	2.1463
SFSF	1	0.6343	0.4561	0.4111	0.4065	0.4055	0.4055
	2	1.0208	0.7488	0.6762	0.6687	0.6671	0.6671
	3	2.0198	1.5619	1.4176	1.4025	1.3993	1.3992
	4	2.1214	1.6203	1.4682	1.4523	1.4490	1.4490
	5	2.2066	1.7005	1.6979	1.6928	1.6904	1.6904

Table 9
The first five non-dimensional frequencies Ω_m of Al/Al_2O_3 square BDFG plate vertically immersed in the water ($a = 1$; $h/a = 0.2$, $p_x = 1$, $p_z = 1$).

BC	Mode	In vacuum	Vertically immersed in water (Z_2/b)				
			0.1	0.3	0.5	0.7	1
CCCC	1	2.0019	1.5858	1.4645	1.3804	1.3233	1.2700
	2	3.5995	2.8302	2.6194	2.4719	2.3711	2.2766
	3	3.6052	2.8610	2.6489	2.5004	2.3989	2.3036
	4	4.7189	3.8563	3.5756	3.3765	3.2399	3.1114
	5	4.7568	3.8764	3.8749	3.7468	3.5951	3.4519
CCCS	1	1.8297	1.4581	1.3474	1.2705	1.2183	1.1694
	2	3.2440	2.5743	2.3865	2.2546	2.1643	2.0794
	3	3.5230	2.8059	2.5987	2.4535	2.3542	2.2610
	4	4.1884	3.6937	3.4301	3.2415	3.1118	2.9895
	5	4.6270	3.7614	3.7377	3.5537	3.4126	3.2789
CSCS	1	1.7050	1.3560	1.2532	1.1819	1.1334	1.0881
	2	2.9258	2.3613	2.1926	2.0738	1.9922	1.9154
	3	3.4726	2.7277	2.5255	2.3840	2.2872	2.1964
	4	3.7028	3.4796	3.3238	3.1433	3.0190	2.9017
	5	4.4600	3.5776	3.4545	3.3585	3.2430	3.1244
CFCF	1	1.3009	1.0405	0.9592	0.9031	0.8652	0.8298
	2	1.5782	1.2736	1.1763	1.1089	1.0631	1.0203
	3	2.2089	1.8264	1.8262	1.7478	1.6790	1.6142
	4	2.4608	1.9908	1.8481	1.8261	1.8260	1.8260
	5	3.1082	2.4749	2.2891	2.1596	2.0712	1.9884
CSSS	1	1.4453	1.1555	1.0688	1.0086	0.9675	0.9291
	2	2.8007	2.2608	2.1002	1.9870	1.9093	1.8360
	3	3.0701	2.4401	2.2634	2.1392	2.0541	1.9741
	4	3.6722	3.3649	3.1303	2.9631	2.8477	2.7386
	5	4.0557	3.4659	3.4346	3.3231	3.2061	3.0884
SFSS	1	0.7594	0.6390	0.5916	0.5587	0.5362	0.5151
	2	1.6694	1.3501	1.2528	1.1846	1.1379	1.0940
	3	2.3161	1.9751	1.8369	1.7394	1.6723	1.6091
	4	2.6122	2.3184	2.3136	2.2540	2.1675	2.0857
	5	3.1025	2.5568	2.3797	2.2903	2.2250	2.1463
SFSF	1	0.6343	0.5070	0.4679	0.4409	0.4226	0.4055
	2	1.0208	0.8304	0.7678	0.7243	0.6947	0.6671
	3	2.0198	1.7009	1.5990	1.5134	1.4546	1.3992
	4	2.1214	1.7205	1.6596	1.5692	1.5072	1.4490
	5	2.2066	1.7886	1.7006	1.7003	1.6997	1.6904

a/hvaries from 5 to 100 in the vacuum, the natural frequency Ω_1 increases with the values $a/h = 5,\ 10$ and it does not much change when the length-to-thickness ratio a/h is larger than 10.

The effects of the length-to-thickness ratio $a/\ h$, the power-law indexes p_x, p_z and the fluid depth level to length ratio $Z_2/\ b$on the natural frequencies $\Omega_1$of the Al/Al_2O_3square BDFG plate (with the SSSS boundary condition) vertically immersed in the water are reported in Table 7. It can be observed that the increase of fluid depth level to length ratio Z_2/bmakes the natural frequency $\Omega_1$decrease continuously until the vertical plate is completely submerged in the water. It is noted that the natural frequency $\Omega_1$are the same when the vertical plate and the horizontal plate are completely submerged in the water.

Table 8 and Table 9 present, respectively, the influence of the boundary conditions: CCCC, CCCS, CSCS, CFCF, SSSC, SFSS, and SFSF on the first five frequencies of the plate horizontal submerged in the water (h_1/a) and the plate vertical partially in contact with the fluid Z_2/b . Similar to the behavior of plates in a vacuum, the natural frequency $\Omega_1$of the plates submerged in the water gains the maximum value with the CCCC boundary condition and the minimum value with the SFSF boundary condition.

Fig. 6 and Fig. 7 depicted, respectively, the first six modes of the Al/Al_2O_3square BDFG (with the SSSS boundary condition) plate horizontally submerged in the water and of the Al/ Al_2O_3square BDFG (with the SFSF boundary condition) plate vertically immersed in the water. It can be seen that similar to plate structures in vacuum or air, the results of the shapes and values of modes 2 and 3 are similar in the SSSS boundary conditions. This phenomenon is also the same for the modes 5 and 6. Fig. 8 illustrate the effect of the length to thickness on the dimensionless natural frequency Ω_1 of BDFG plates in contact with the fluid. From Fig. 8, it can be observed that when the length to thickness ratio $a/h = 2$, the natural frequency $\Omega_1$in vacuum and fluid are the same. However, when the length to thickness ratio of the plate increases, the natural frequency of the plate in vacuum increases to a maximum value and then decreases for the plates submerged in fluid and the attenuation rate of the horizontal plate is faster than the vertical plate in the fluid medium. Moreover, the vertical plate in the fluid has a higher value of the natural frequency than those of the horizontal plate in the fluid.

The effects of the width-to-length ratio b/aon the natural frequency Ω_1 of the BDFG plates are plotted in Fig. 9. It can be observed that the length to width ratio b/a changing from 0.5 to 3 makes the natural frequency Ω_1 increase rapidly in all three cases: plate in a vacuum, plate horizontally submerged in the water and plate vertically submerged in the water. In addition, when the ratio b/a is larger, the difference between the natural frequency of horizontal and vertical plates in the fluid medium also become larger. However, the horizontal plate in the fluid medium always gives a smaller natural frequency.

The influence of the power-law indexes p_x, p_zon the natural frequency Ω_1 of the BDFG plates are plotted in Fig. 10. It can be seen that the natural frequency decreases rapidly when the power-law indexes p_x, p_zvary from 0 to 2, however, those decrease slowly

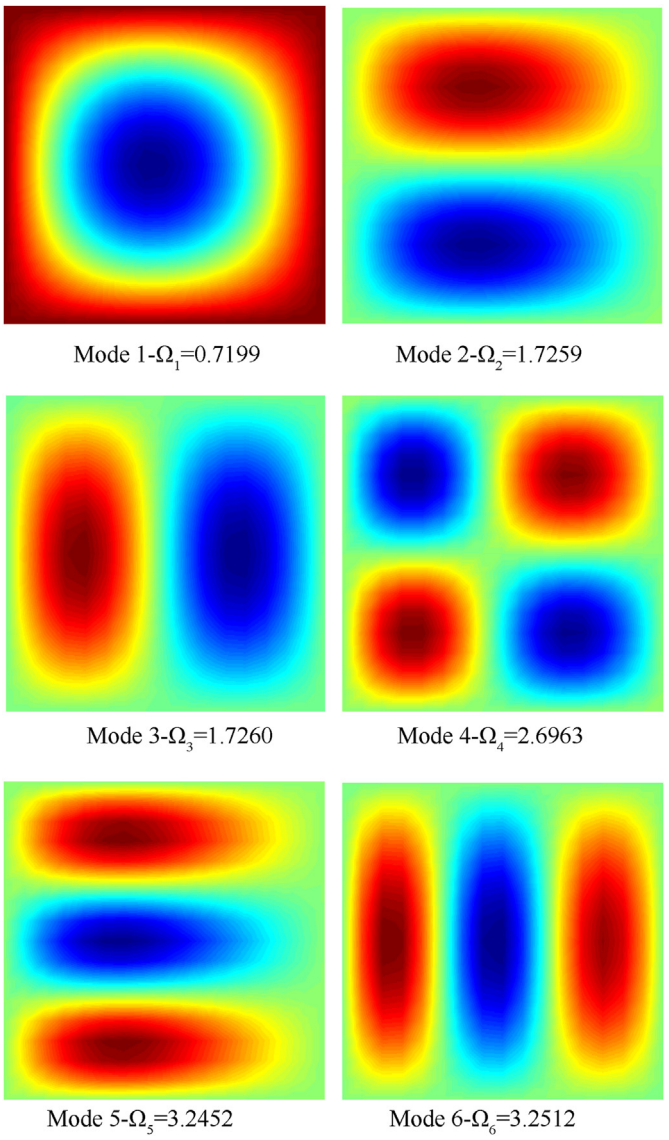

Fig. 6. The first six free vibration modes of the Al/Al_2O_3 square BDFG plate (with the SSSS boundary condition) horizontally submerged in the water ($a = 1$; $h/a = 0.1$, $p_x = 1$, $p_z = 1, h_1 = 0.5a$).

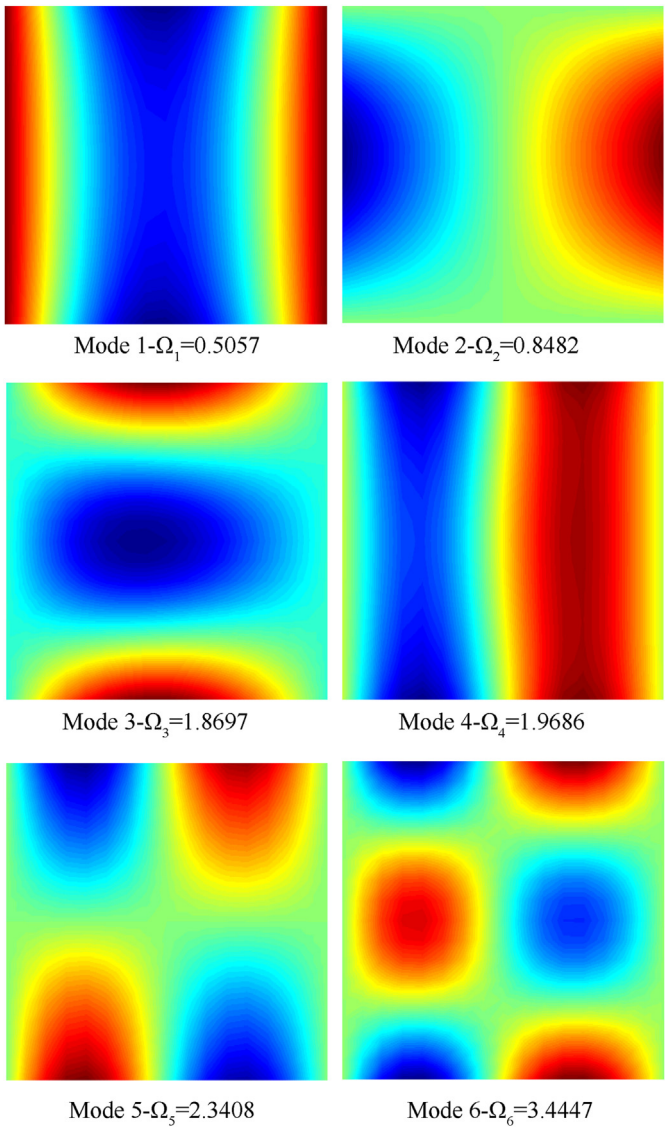

Fig. 7. The first six free vibration modes of the Al/Al_2O_3 square BDFG plate (with the SFSF boundary condition) vertically immersed in the water ($a = 1$; $h/a = 0.1$, $p_x = 1$, $p_z = 1, Z_2 = 0.5b$).

when the power-law indexes p_x, p_z are larger than 2 because the plate in this case almost only contains the metal. The effects of the submerged distance $d_1 (d_1 = 0.1 - 1.1$ m) in the fluid of the vertical BDFG plate on the natural frequency are displayed in Fig. 11 and Fig. 12. From Fig. 11 which presents the x-direction FGM plate ($p_x = 1$, $p_z = 0$), the z-direction FGM plate ($p_x = 0$, $p_z = 1$) and bidirectional FGM plate ($p_x = 1$, $p_z = 2$ & $p_x = 2$, $p_z = 1$) partially submerged in fluid ($Z_2 = 0.3b$), it is found that when the submerged distance of the plate d_1 changes from 0.1 to 0.2 m, the natural frequency Ω_1 increases. However, when the submerged distance of the plate is higher than 2 m ($d_1 > 0.2$ m), the natural frequency Ω_1 does not change and it progresses to a fixed value. This may be explained that when the submerged depth of plate in fluid ($d_1 > 0.2$ m) the value of added mass $m_{add} = 2\frac{\rho_f}{\gamma}$ (constant) is constant and hence the natural frequency Ω_1 does not change. The concurrent effects of submerged level Z_2 and the submerged depth of plate in fluid d_1 on the natural frequency Ω_1 are depicted in Fig. 12. From the figure, it is seen that if the level of submerged in a fluid is low $Z_2 = 0.1b$, the increase of submerged distance d_1 does not have much effect on the natural frequency Ω_1. However, when the submerged level Z_2 increases until to the value of b ($Z_2 = b$), the

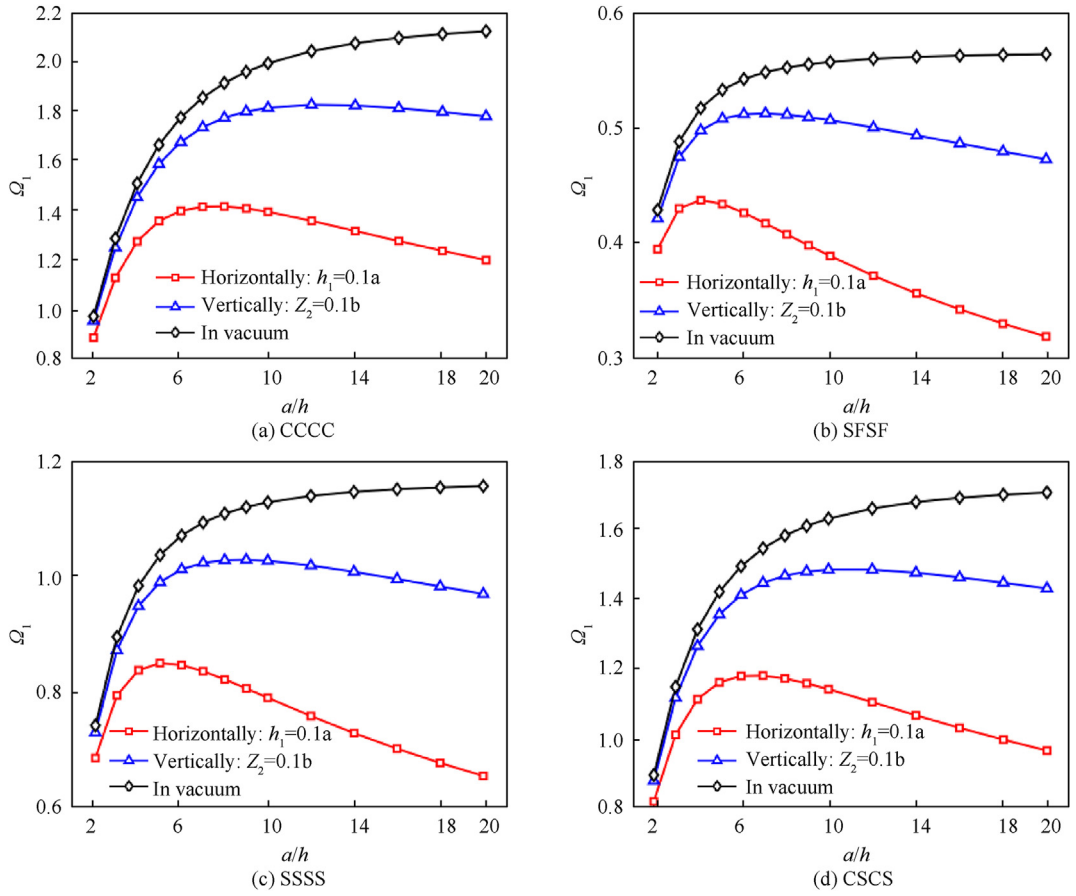

Fig. 8. Effect of the various length to thickness ratio a/hon the dimensionless natural frequency Ω_1 of the Al/Al_2O_3 square BDFG plate $(a = 1,\ p_x = 1,\ p_z = 1, d_2 = d_1)$with different boundary conditions: a) CCCC; b) SFSF; c) SSSS; d) CSCS.

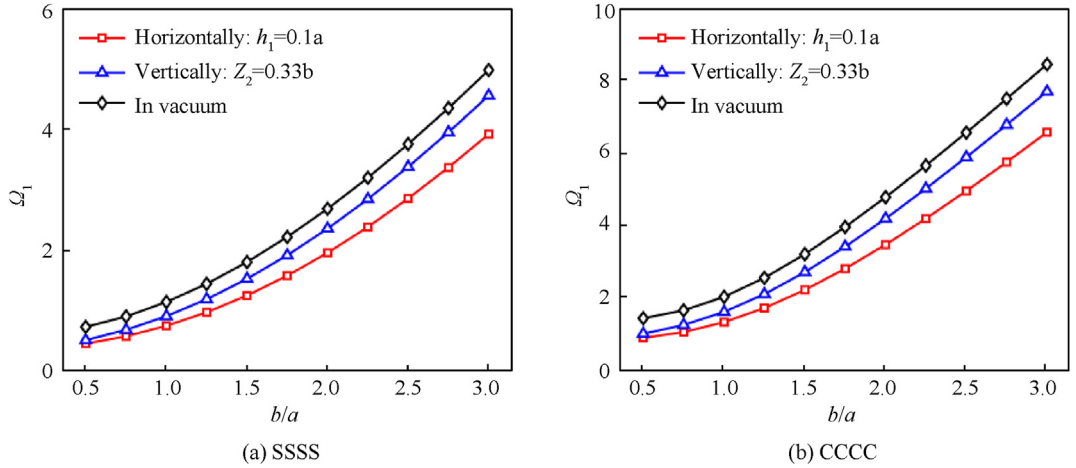

Fig. 9. Effects of the width-to-length ratio b/a on the dimensionless natural frequency $\Omega_1$of the Al/Al_2O_3BDFG plate $(a = 1, h/a = 0.1, d_2 = d_1)$with different boundary conditions: a) SSSS; b) CCCC.

increase of submerged depth of the plate $d_1$significantly affects the natural frequency. Ω_1.

Finally, the influence of the fluid density $\rho_f$on the natural frequency $\Omega_1$is plotted in Fig. 13. As observed from figure, the greater the fluid density $\rho_f$increases, the lower the natural frequency $\Omega_1$becomes. In particular, the horizontal plate partially submerged in fluid has a very rapid reduction in natural frequency, with $\rho_f = 1200 kg/m^3$ and Al/Al_2O_3 the natural frequency decrease 33.04%; and with $Al/ZrO_2$the natural frequency decrease 35.6%. The reduction law of the natural frequency of the vertical plate is almost linear according to change of the fluid density ρ_f, while this law of the horizontally plate is almost nonlinear.

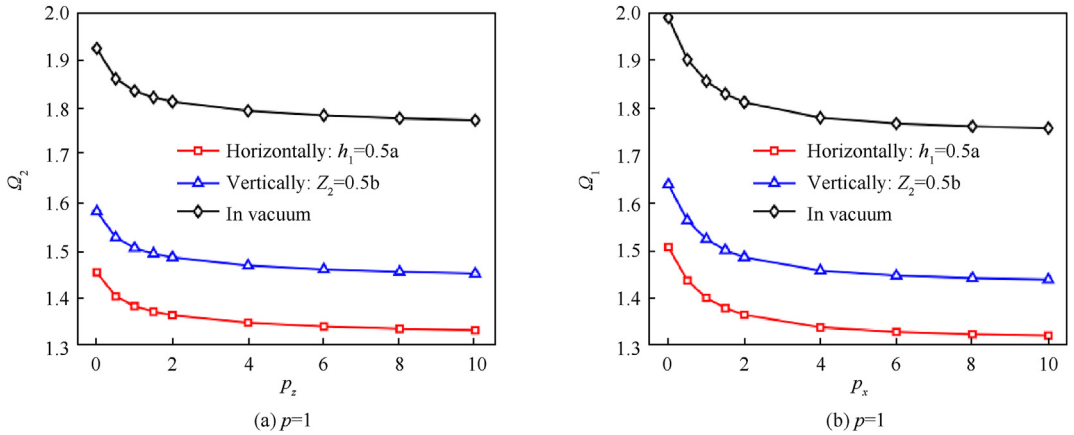

Fig. 10. Effects of the power-law indexes p_x, p_z on the dimensionless natural frequency $\Omega_1$of the Al/Al_2O_3square BDFG plate $(a = 1, h/a = 0.1, d_2 = d_1)$ with the CSCS boundary condition.

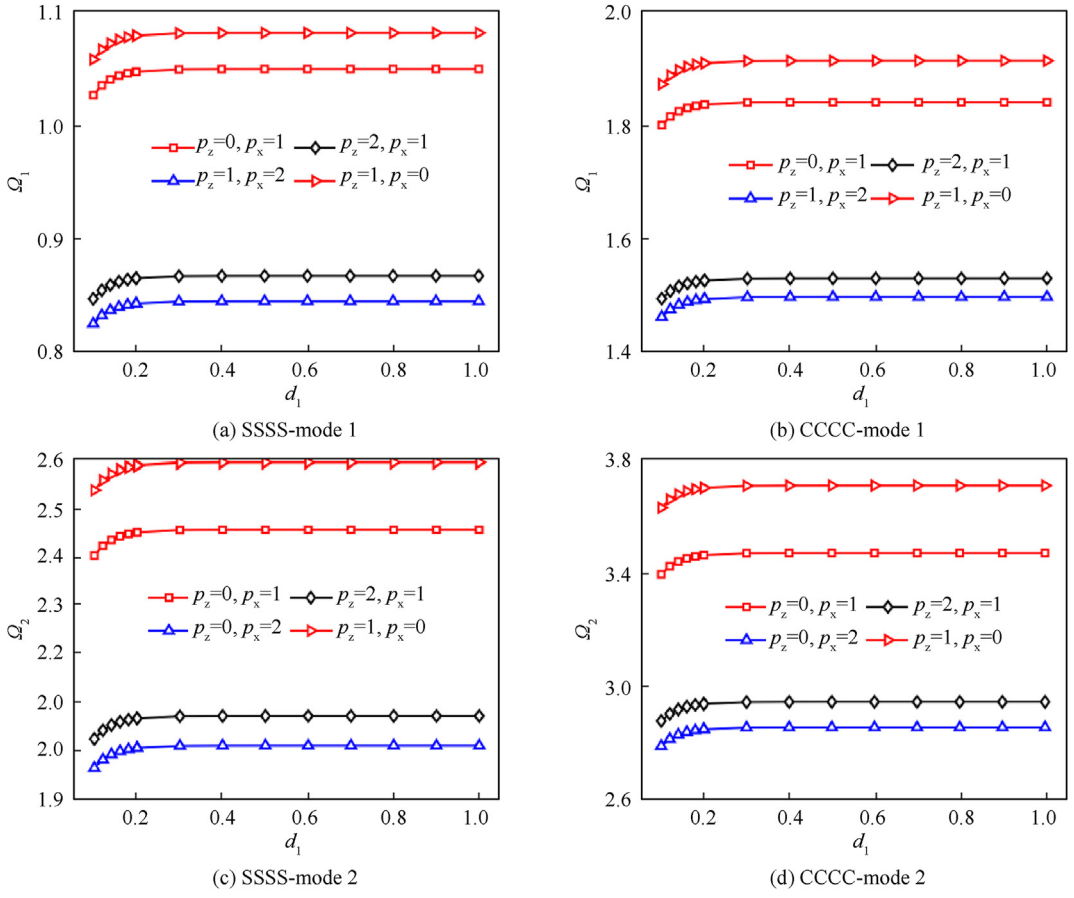

Fig. 11. Effects of the submerged distance d_1 in fluid on the dimensionless natural frequency Ω_m of the Al/Al_2O_3 square BDFG plate $(a = 1;\ h/a = 0.1, Z_2 = 0.3b)$.

5. Conclusion

The present work presented an isogeometric analysis (IGA) for free vibration response of bi-directional functionally graded (BDFG) rectangular plates in the fluid medium. Material properties of the BDFG plate change in both the thickness and length directions via power-law distributions. The proposed method is based on Hamilton's principle and the refined quasi 3D plate theory to obtain the governing equation of motion of the BDFG plate. The horizontal and vertical BDFG plates are partially submerged or completely submerged in the fluid, which is considered homogeneous, incompressible, inviscid and has no rotation. The variations of Young's modulus, Poisson's ratio is derived by the Mori-Tanaka model and mass density is obtained by the Voigt model. The accuracy and reliability of the proposed solutions are verified by comparing the obtained results with those published in the literature. In addition,

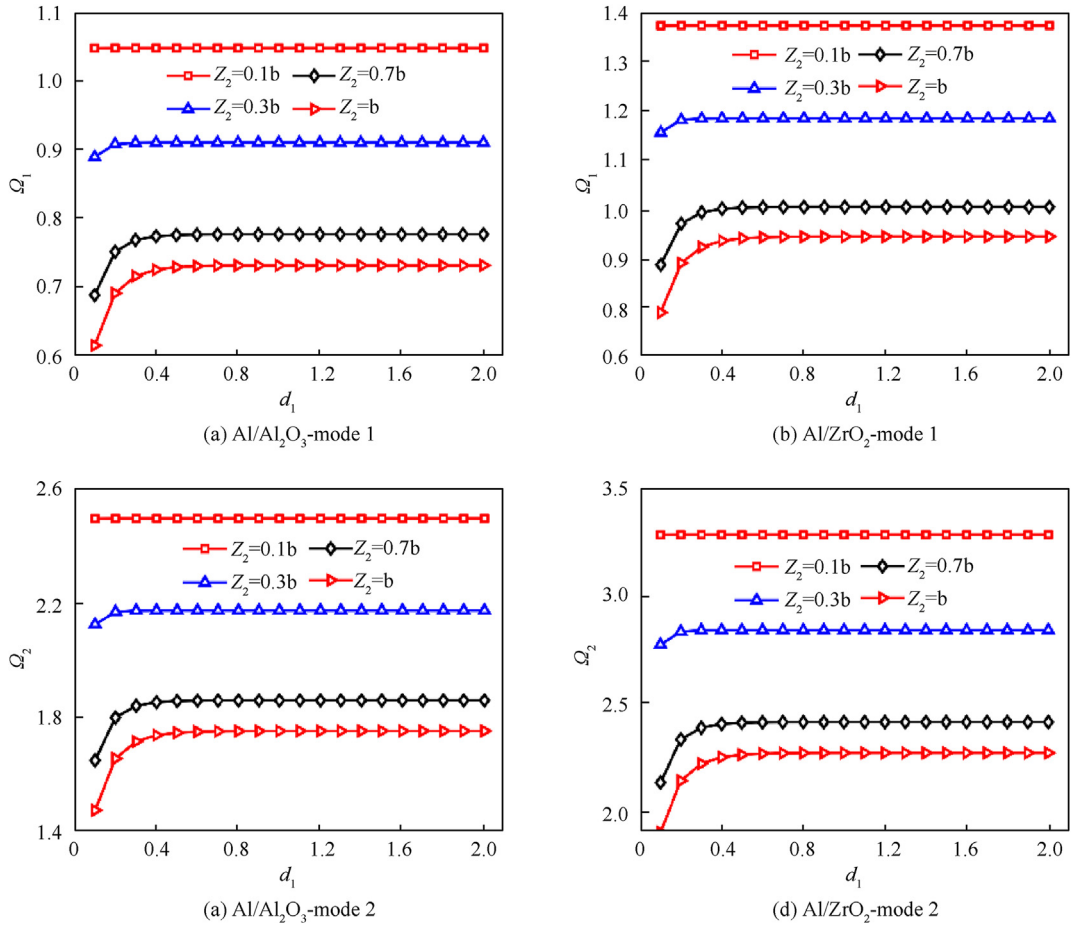

Fig. 12. Effects of the submerged distance d_1 in fluid on the first two dimensionless natural frequency Ω_m of the Al/Al2O3and the Al/ZrO2square BDFG plate (with the SSSS boundary condition) partially submerged in fluid.($a = 1;\ h/a = 0.1, p_x = 0.5,\ p_z = 2$).

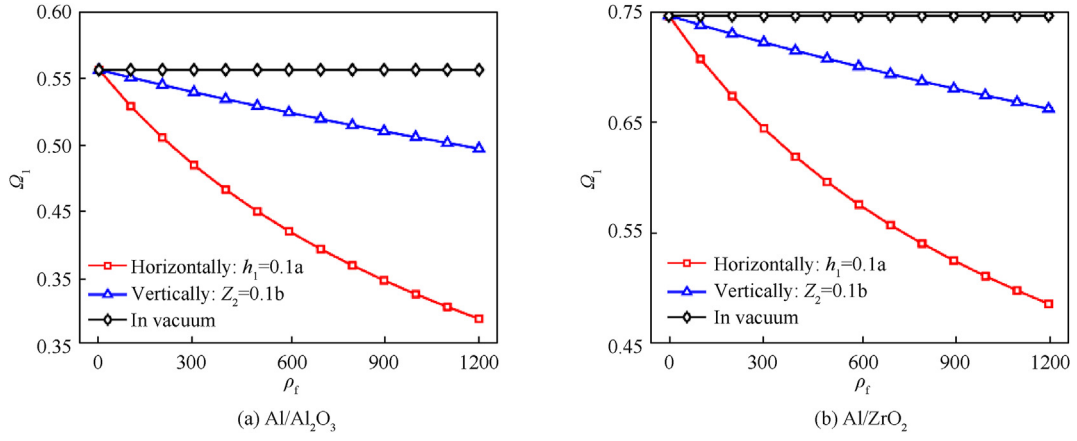

Fig. 13. Effects of the fluid mass density $\rho_f$on the dimensionless natural frequency $\Omega_1$of the Al/Al$_2$O$_3$ and the Al/ZrO$_2$square BDFG plate.($a = 1;\ h/a = 0.1, p_x = 1,\ p_z = 1, d_2 = d_1$).

based on the numerical studies, some additional points are withdrawn as follows:

- When the submerged level in the fluid of the BDFG plate Z_2increases, the natural frequency Ω_1 decreases. However, when the submerged level in the fluid of the BDFG plate Z_2increases to $h_1 = a,\ Z_2 = b$, the natural frequency $\Omega_1$does not change.
- The increase of the length-to-thickness ratio $(a/h)$of the BDFG plates submerged in fluid leads to the increase of the natural frequency Ω_1 to a maximum value, and then to a decrease. While the increase of the length-to-thickness ratio $(a/h)$of the BDFG plate in a vacuum only leads to the increase of the natural frequency Ω_1.

- The increase of the width-to-length ratio $b/a$of the BDFG plates submerged in fluid gives the changing law of the natural frequency Ω_1 similar to the changing law of the BDFG plate in a vacuum.
- The increase of the power-law indexes p_x, p_z or the increase of fluid mass density $\rho_f$makes the natural frequency $\Omega_1$decrease. For the BDFG plate partially submerged in fluid, the increase of the submerged distance d_1 leads to the increase of the natural frequency Ω_1, however, it only increases to a certain value and then is almost unchanged.

Data availability

The data used to support the findings of this study are included in the article.

Declaration of competing interest

The authors declare that they have no known competing financial interests or personal relationships that could have appeared to influence the work reported in this paper.

Acknowledgements

This research is funded by Vietnam National Foundation for Science and Technology Development (NAFOSTED) under Grant number 107.02-2019.330.

References

[1] Nguyen-Xuan H, Tran LV, Nguyen-Thoi T, Vu-Do HC. Analysis of functionally graded plates using an edge-based smoothed finite element method. Compos Struct 2011;93(11):3019–39. https://doi.org/10.1016/j.compstruct.2011.04.028.

[2] Phung-Van P, Nguyen-Thoi T, Tran LV, Nguyen-Xuan H. A cell-based smoothed discrete shear gap method (CS-DSG3) based on the C0-type higher-order shear deformation theory for static and free vibration analyses of functionally graded plates. Comput Mater Sci 2013;79:857–72. https://doi.org/10.1016/j.commatsci.2013.06.010.

[3] Phung-Van P, Nguyen-Thoi T, Luong-Van H, Lieu-Xuan Q. Geometrically nonlinear analysis of functionally graded plates using a cell-based smoothed three-node plate element (CS-MIN3) based on the C0–HSDT. Comput Methods Appl Math 2014;270:15–36. https://doi.org/10.1016/j.cma.2013.11.019.

[4] Tahir SI, Tounsi A, Chikh A, Al-Osta MA, Al-Dulaijan SU, Al-Zahrani MM. An integral four-variable hyperbolic HSDT for the wave propagation investigation of a ceramic-metal FGM plate with various porosity distributions resting on a viscoelastic foundation. Wave Random Complex 2021. https://doi.org/10.1080/17455030.2021.1942310.

[5] Tahir SI, Chikh A, Tounsi A, Al-Osta MA, Al-DulaijanMesfer SU, Al-Zahrani MM. Wave propagation analysis of a ceramic-metal functionally graded sandwich plate with different porosity distributions in a hygro-thermal environment. Compos Struct 2021;269:114030. https://doi.org/10.1016/j.compstruct.2021.114030.

[6] Menasria A, Kaci A, Bousahla AA, Bourada F, Tounsi A, Benrahou KH, Tounsi A, Bedia EA, Mahmoud SR. A four-unknown refined plate theory for dynamic analysis of FG-sandwich plates under various boundary conditions. Steel Compos Struct 2020;36(3):355–67. https://doi.org/10.12989/scs.2020.36.3.355.

[7] Chakraverty S, Pradhan KK. Free vibration of exponential functionally graded rectangular plates in thermal environment with general boundary conditions. Aero Sci Technol 2014;36:132–56. https://doi.org/10.1016/j.ast.2014.04.005.

[8] Zaoui FZ, Ouinas D, Tounsi A. New 2D and quasi-3D shear deformation theories for free vibration of functionally graded plates on elastic foundations. Compos B Eng 2019;159:231–47. https://doi.org/10.1016/j.compositesb.2018.09.051.

[9] Karami B, Shahsavari D, Janghorban M. A comprehensive analytical study on functionally graded carbon nanotube-reinforced composite plates. Aero Sci Technol 2018;82–83:499–512. https://doi.org/10.1016/j.ast.2018.10.001.

[10] Mudhaffar IM, Tounsi A, Chikh A, Al-Osta MA, Al-Zahrani MM, Al-Dulaijan SU. Hygro-thermo-mechanical bending behavior of advanced functionally graded ceramic metal plate resting on a viscoelastic foundation. Structure 2021;33:2177–89. https://doi.org/10.1016/j.istruc.2021.05.090.

[11] Merazka B, Bouhadra A, Menasria A, Selim MM, Bousahla AA, Bourada F, Tounsi A, Halim Benrahou Kouider, Tounsi A, Al-Zahrani MM. Hygro-thermo-mechanical bending response of FG plates resting on elastic foundations. Steel Compos Struct 2021;39(5):631–43. https://doi.org/10.12989/scs.2021.39.5.631.

[12] Bendenia N, Zidour M, Bousahla AA, Bourada F, Tounsi A, Benrahou KH, Bedia EAA, Mahmoud SR, Tounsi A. Deflections, stresses and free vibration studies of FG-CNT reinforced sandwich plates resting on Pasternak elastic foundation. Comput Concr 2020;26(3):213–26. https://doi.org/10.12989/cac.2020.26.3.213.

[13] Hachemi H, Bousahla AA, Kaci A, Bourada F, Tounsi A, Benrahou KH, Tounsi A, Al-Zahrani MM, Mahmoud SR. Bending analysis of functionally graded plates using a new refined quasi-3D shear deformation theory and the concept of the neutral surface position. Steel Compos Struct 2021;39(1):51–64. https://doi.org/10.12989/scs.2021.39.1.051.

[14] Bakoura A, Bourada F, Bousahla AA, Tounsi A, Benrahou KH, Tounsi A, Al-Zahrani MM, Mahmoud SR. Buckling analysis of functionally graded plates using HSDT in conjunction with the stress function method. Comput Concr 2021;27(1):73–83. https://doi.org/10.12989/cac.2021.27.1.073.

[15] Bekkaye THL, Fahsi B, Bousahla AA, Bourada F, Tounsi A, Benrahou KH, Tounsi A, Al-Zahrani MM. Porosity-dependent mechanical behaviors of FG plate using refined trigonometric shear deformation theory. Comput Concr 2020;26(5):439–50. https://doi.org/10.12989/cac.2020.26.5.439.

[16] Rezaei AS, Saidi AR, Abrishamdari M, Pour-Mohammadi MH. Natural frequencies of functionally graded plates with porosities via a simple four variable plate theory, an analytical approach. Thin-Walled Struct 2017;120:366–77. https://doi.org/10.1016/j.tws.2017.08.003.

[17] Li M, Guedes Soares C, Yan R. A novel shear deformation theory for static analysis of functionally graded plates. Compos Struct 2020;250:112559. https://doi.org/10.1016/j.compstruct.2020.112559.

[18] Nguyen NV, Nguyen-Xuan H, Lee D, Lee J. A novel computational approach to functionally graded porous plates with graphene platelets reinforcement. Thin-Walled Struct 2020;150:106684. https://doi.org/10.1016/j.tws.2020.106684.

[19] Naveen Kumar HS, Kattimani Subhaschandra, Nguyen-Thoi T. Influence of porosity distribution on nonlinear free vibration and transient responses of porous functionally graded skew plates. Def Technol 2021. https://doi.org/10.1016/j.dt.2021.02.003.

[20] Tran TT, Pham QH, Nguyen-Thoi T. Static and free vibration analyses of functionally graded porous variable-thickness plates using an edge-based smoothed finite element method. Def Technol 2021;17:971–86. https://doi.org/10.1016/j.dt.2020.06.001.

[21] Tran TT, Pham QH, Nguyen-Thoi T. An edge-based smoothed finite element for free vibration analysis of functionally graded porous FGP plates on elastic foundation taking into mass EFTIM. Math Probl Eng 2020;2020:1–17. https://doi.org/10.1155/2020/8278743.

[22] Tran TT, Pham QH, Nguyen-Thoi T. Dynamic analysis of functionally graded porous plates resting on elastic foundation taking into mass subjected to moving loads using an edge-based smoothed finite element method. Shock Vib 2020;2020:1–19. https://doi.org/10.1155/2020/8853920.

[23] Pham QH, PhamTD, Trinh QV, Phan DH. Geometrically nonlinear analysis of functionally graded shells using an edge-based smoothed MITC3 ES-MITC3 finite elements. Eng Comput-Germany 2019;36:1069–82. https://doi.org/10.1007/s00366-019-00750-z.

[24] Tran TV, Tran TD, Pham QH, Nguyen-Thoi T, Tran VK. An ES-MITC3 finite element method based on higher-order shear deformation theory for static and free vibration analyses of FG porous plates reinforced by GPLs. Math Probl Eng 2020:1–18. https://doi.org/10.1155/2020/7520209.

[25] Karamanlı A, Vo TP. Size dependent bending analysis of two directional functionally graded microbeams via a quasi-3D theory and finite element method. Compos B Eng 2018;144:171–83. https://doi.org/10.1016/j.compositesb.2018.02.030.

[26] Li S, Zheng S, Chen D. Porosity-dependent isogeometric analysis of bi-directional functionally graded plates. Thin-Walled Struct 2020;156:106999. https://doi.org/10.1016/j.tws.2020.106999.

[27] Lieu QX, Lee S, Kang J, Lee J. Bending and free vibration analyses of in-plane bi-directional functionally graded plates with variable thickness using isogeometric analysis. Compos Struct 2018;192:434–51. https://doi.org/10.1016/j.compstruct.2018.03.021.

[28] Lieu QX, Lee S, Kang J, Lee J. NURBS-based modeling and analysis for free vibration and buckling problems of in-plane bi-directional functionally graded plates. Mech Adv Mater Struct 2019;26(12):1064–80. https://doi.org/10.1080/15376494.2018.1430273.

[29] Wu CP, Yu LT. Free vibration analysis of bi-directional functionally graded annular plates using finite annular prism methods. J Mech Sci Technol 2019;33(5):2267–79. https://doi.org/10.1007/s12206-019-0428-5.

[30] Cho DS, Kim BH, Vladimir N, Choi TM. Natural vibration analysis of vertical rectangular plates and stiffened panels in contact with fluid on one side. Proc IME M J Eng Marit Environ 2014;230(1):114–25. https://doi.org/10.1177/1475090214533955.

[31] Cho DS, Kim BH, Vladimir N, Choi TM. Frequency response of rectangular plate structures in contact with fluid subjected to harmonic point excitation force. Thin-Walled Struct 2015;95:276–86. https://doi.org/10.1016/j.tws.2015.07.013.

[32] Hosseini-Hashemi S, Karimi M, Rokni Damavandi Taher H. Vibration analysis of rectangular Mindlin plates on elastic foundations and vertically in contact

with stationary fluid by the Ritz method. Ocean Eng 2010;37(2–3):174–85. https://doi.org/10.1016/j.oceaneng.2009.12.001.
[33] Watts G, Pradyumna S, Singha MK. Free vibration analysis of non-rectangular plates in contact with bounded fluid using element free Galerkin method. Ocean Eng 2018;160:438–48. https://doi.org/10.1016/j.oceaneng.2018.04.056.
[34] Bendahmane A, Hamza-Cherif SM, Ouissi MN. Free vibration analysis of variable stiffness composite laminate VSCL plates coupled with fluid. Mech Adv Mater Struct 2019;28(2):167–81. https://doi.org/10.1080/15376494.2018.1553257.
[35] Khorshid K, Farhadi S. Free vibration analysis of a laminated composite rectangular plate in contact with a bounded fluid. Compos Struct 2013;104:176–86. https://doi.org/10.1016/j.compstruct.2013.04.005.
[36] Khorshidi K, Bakhsheshy A. Free vibration analysis of a functionally graded rectangular plate in contact with a bounded fluid. Acta Mech 2015;226(10):3401–23. https://doi.org/10.1007/s00707-015-1368-5.
[37] Khorshidi K, Akbari F, Ghadirian H. Experimental and analytical modal studies of vibrating rectangular plates in contact with a bounded fluid. Ocean Eng 2017;140:146–54. https://doi.org/10.1016/j.oceaneng.2017.05.017.
[38] Hughes TJR, Cottrell JA, Bazilevs Y. Isogeometric analysis, CAD, finite elements, NURBS, exact geometry and mesh refinement. Comput Methods Appl Math 2005;194(39–41):4135–95. https://doi.org/10.1016/j.cma.2004.10.008.
[39] Cazzani A, Malagu M, Turco E, Stochino F. Constitutive models for strongly curved beams in the frame of isogeometric analysis. Math Mech Solid 2015;212:182–209. https://doi.org/10.1177/1081286515577043.
[40] Balobanov V, Niiranen J. Locking-free variational formulations and isogeometric analysis for the Timoshenko beam models of strain gradient and classical elasticity. Comput Methods Appl Math 2018;339:137–59. https://doi.org/10.1016/j.cma.2018.04.028.
[41] Fang W, Yu T, Lich LV, Bui QT. Analysis of thick porous beams by a quasi-3D theory and isogeometric analysis. Compos Struct 2019;221:110890. https://doi.org/10.1016/j. compstruct.2019.04.062.
[42] Borković A, Kovačević S, Radenković G, Milovanović S, Guzijan-Dilber M. Rotation-free isogeometric analysis of an arbitrarily curved plane Bernoulli–Euler beam. Comput Methods Appl Math 2018;334:238–67. https://doi.org/10.1016/j.cma.2018.02.002.
[43] Yan Y, Carrera E, Pagari A, Kaleel I, Miguel ADd. Isogeometric analysis of 3D straight beam-type structures by Carrera Unified Formulation. Appl Math Model 2020;79:768–92. https://doi.org/10.1016/j.apm.2019.11.003.
[44] Radenković G, Borković A. Linear static isogeometric analysis of an arbitrarily curved spatial Bernoulli–Euler beam. Comput Methods Appl Math 2018;341:360–96. https://doi.org/10.1016/j.cma.2018.07.010.
[45] Vo D, Nanakorn P. Geometrically nonlinear multi-patch isogeometric analysis of planar curved Euler–Bernoulli beams. Comput Methods Appl Math 2020;366:113078. https://doi.org/10.1016/j.cma.2020.113078.
[46] Truong TT, Nguyen-Thoi T, Lee J. Isogeometric size optimization of bi-directional functionally graded beams under static loads. Compos Struct 2019;227:111259. https://doi.org/10.1016/j.compstruct.2019.111259.
[47] Nguyen-Xuan H, Thai CH, Nguyen-Thoi T. Isogeometric finite element analysis of composite sandwich plates using a higher order shear deformation theory. Compos B Eng 2013;55:558–74. https://doi.org/10.1016/j.compositesb.2013.06.044.
[48] Nguyen-Quang H, Vo-Duy T, Dang-Trung H, Nguyen-Thoi T. An isogeometric approach for dynamic response of laminated FG-CNT reinforced composite plates integrated with piezoelectric layers. Comput Methods Appl Math 2018;332:25–46. https://doi.org/10.1016/j.cma.2017.12.010.
[49] Farzam-Rad SA, Hassani B, Karamodin A. Isogeometric analysis of functionally graded plates using a new quasi-3D shear deformation theory based on physical neutral surface. Compos B Eng 2017;108:174–89. https://doi.org/10.1016/j.compositesb.2016.09.029.
[50] Hien TD, Noh HC. Stochastic isogeometric analysis of free vibration of functionally graded plates considering material randomness. Comput Methods Appl Math 2017;318:845–63. https://doi.org/10.1016/j.cma.2017.02.007.
[51] Li K, Wu D, Chen X, Cheng J, Liu Z, Gao Z, Liu M. Isogeometric Analysis of functionally graded porous plates reinforced by graphene platelets. Compos Struct 2018;204:114–30. https://doi.org/10.1016/j.compstruct.2018.07.059.
[52] Thai CH, Zenkour AM, Abdel Wahab M, Nguyen-Xuan H. A simple four-unknown shear and normal deformations theory for functionally graded isotropic and sandwich plates based on isogeometric analysis. Compos Struct 2016;139:77–95. https://doi.org/10.1016/j.compstruct.2015.11.066.
[53] Tran LV, Phung-Van P, Lee J, Abdel Wahab M, Nguyen-Xuan H. Isogeometric analysis for nonlinear thermomechanical stability of functionally graded plates. Compos Struct 2016;140:655–67. https://doi.org/10.1016/j.compstruct.2016.01.001.
[54] Yu T, Yin S, Bui QT, Liu C, Wattanasakulpong N. Buckling isogeometric analysis of functionally graded plates under combined thermal and mechanical loads. Compos Struct 2017;162:54–69. https://doi.org/10.1016/j.compstruct.2016.11.084.
[55] Zhu Y, Shi P, Kang Y, Cheng B. Isogeometric analysis of functionally graded plates with a logarithmic higher order shear deformation theory. Thin-Walled Struct 2019;144:106234. https://doi.org/10.1016/j.tws.2019.106234.
[56] Kiendl J, Blezinger KU, Linhard J, Wüchner R. Isogeometric shell analysis with Kirchhoff–Love elements. Comput Methods Appl Math 2009;198(49–52):3902–14. https://doi.org/10.1016/j.cma.2009.08.013.
[57] Nguyen TN, Zhou K, Zhuang X, Areias P, Nguyen-Xuan H, Bazilevs Y, Rabczuk T. Isogeometric analysis of large-deformation thin shells using RHT-splines for multiple-patch coupling. Comput Methods Appl Math 2017;316:1157–78. https://doi.org/10.1016/j.cma.2016.12.002.
[58] Benson DJ, Bazilevs Y, Hsu MC, Hughes TJR. Isogeometric shell analysis, the Reissner–Mindlin shell. Comput Methods Appl Math 2010;199(5–8):276–89. https://doi.org/10.1016/j.cma.2009.05.011.
[59] Coradello L, D'Angella, Carraturo M, Kiendl J, Kollmannsberger S, Rank E, Reali A. Hierarchically refined isogeometric analysis of trimmed shells. Comput Mech 2020;66(2):431–47. https://doi.org/10.1007/s00466-020-01858-6.
[60] Schuß S, Dittmann M, Wohlmuth B, Klinkel S, Hesch C. Multi-patch isogeometric analysis for Kirchhoff–Love shell elements. Comput Methods Appl Math 2019;349:91–116. https://doi.org/10.1016/j.cma.2019.02.015.
[61] Zareh M, Qian X. Kirchhoff–Love shell formulation based on triangular isogeometric analysis. Comput Methods Appl Math 2019;347:853–73. https://doi.org/10.1016/j.cma.2018.12.034.
[62] Schulte J, Dittmann M, Eugster SR, Hesch S, Reinicke T, dell'Isola F, Hesch C. Isogeometric analysis of fiber reinforced composites using Kirchhoff–Love shell elements. Comput Methods Appl Math 2020;362:112845. https://doi.org/10.1016/j.cma.2020.112845.
[63] Nguyen TN, Lee S, Nguyen PC, Nguyen-Xuan H, Lee J. Geometrically nonlinear postbuckling behavior of imperfect FG-CNTRC shells under axial compression using isogeometric analysis. Eur J Mech Solid 2020;84:104066. https://doi.org/10.1016/j.euromechsol.2020.104066.
[64] Norouzzadeh A, Ansari R, Rouhi H. Pre-buckling responses of Timoshenko nanobeams based on the integral and differential models of nonlocal elasticity, an isogeometric approach. Appl Phys A-Mater 2017;123(5):330. https://doi.org/10.1007/s00339-017-0887-4.
[65] Norouzzadeh A, Ansari R, Rouhi H. Nonlinear bending analysis of nanobeams based on the nonlocal strain gradient model using an isogeometric finite element approach. Ijst-T Civ Eng 2018;43(1):533547. https://doi.org/10.1007/s40996-018-0184-2.
[66] Phung-Van P, Thanh CL, Nguyen-Xuan H, Abdel-Wahab M. Nonlinear transient isogeometric analysis of FG-CNTRC nanoplates in thermal environments. Compos Struct 2018;201:882–92. https://doi.org/10.1016/j.compstruct.2018.06.087.
[67] Phung-Van P, Lieu QX, Ferreira AJM, Thai CH. Size-dependent isogeometric analysis of functionally graded carbon nanotube-reinforced composite nanoplates. Compos Struct 2017;166:120–35. https://doi.org/10.1016/j.tws.2021.107862.
[68] Liu S, Yu T, Lich LV, Yin S, Bui QT. Size and surface effects on mechanical behavior of thin nanoplates incorporating microstructures using isogeometric analysis. Comput Struct 2019;212:173–87. https://doi.org/10.1016/j.compstruc.2018.10.009.
[69] Phung-Van P, Thai CH, Nguyen-Xuan H, Abdel-Wahab M. Porosity-dependent nonlinear transient responses of functionally graded nanoplates using isogeometric analysis. Compos B Eng 2019;164:215–25. https://doi.org/10.1016/j.compositesb.2018.11.036.
[70] Phung-Van P, Ferreira AJM, Thai CH. Computational optimization for porosity-dependent isogeometric analysis of functionally graded sandwich nanoplates. Compos Struct 2020;239:112029. https://doi.org/10.1016/j.compstruct.2020.112029.
[71] Thai S, Thai HT, Vo TP, Lee S. Postbuckling analysis of functionally graded nanoplates based on nonlocal theory and isogeometric analysis. Compos Struct 2018;201:13–20. https://doi.org/10.1016/j.compstruct.2018.05.116.
[72] Thanh CL, Phung-Van P, Thai CH, Nguyen-Xuan H, Abdel-Wahab M. Isogeometric analysis of functionally graded carbon nanotube reinforced composite nanoplates using modified couple stress theory. Compos Struct 2018;184:633–49. https://doi.org/10.1016/j. compstruct.2017.10.025.
[73] Fan F, Safaei B, Sahmani S. Buckling and postbuckling response of nonlocal strain gradient porous functionally graded micro/nano-plates via NURBS-based isogeometric analysis. Thin-Walled Struct 2021;159:107231. https://doi.org/10.1016/j.tws.2020.107231.
[74] Banh-Thien T, Dang-Trung H, Le-Anh L, Ho-Huu V, Nguyen-Thoi T. Buckling analysis of non-uniform thickness nanoplates in an elastic medium using the isogeometric analysis. Compos Struct 2017;162:182–93. https://doi.org/10.1016/j.compstruct.2016.11.092.
[75] Tao C, Dai T. Isogeometric analysis for postbuckling of sandwich cylindrical shell panels with graphene platelet reinforced functionally graded porous core. Compos Struct 2021;260:113258. https://doi.org/10.1016/j.compstruct.2020.113258.
[76] Norouzzadeh A, Ansari R. On the isogeometric analysis of geometrically nonlinear shell structures with the consideration of surface energies. Eur Phys J Plus 2020;135(2). https://doi.org/10.1140/epjp/s13360-020-00257-3.
[77] Mori T, Tanaka K. Average stress in matrix and average elastic energy of materials with misfitting inclusions. Acta Metall 1973;21(5):571–4. https://doi.org/10.1016/0001-6160(73)90064-3.
[78] Mantari JL, Guedes Soares C. Five-unknowns generalized hybrid-type quasi-3D HSDT for advanced composite plates. Appl Math Model 2015;39(18):5598–615. https://doi.org/10.1016/j.apm.2015.01.020.
[79] Soni S, Jain NK, Joshi PV. Vibration analysis of partially cracked plate submerged in fluid. J Sound Vib 2018;412:28–57. https://doi.org/10.1016/j.jsv.2017.09.016.
[80] Kerboua Y, Lakis AA, Thomas M, Marcouiller L. Vibration analysis of rectangular plates coupled with fluid. Appl Math Model 2008;32(12):2570–86. https://doi.org/10.1016/j.apm.2007.09.004.

[81] Haddara MR, Cao S. A study of the dynamic response of submerged rectangular flat plates. Mar Struct 1996;9(10):913–33. https://doi.org/10.1016/0951-8339(96)00006-8.
[82] Nguyen XH, Nguyen TN, Abdel-Wahab M, Bordas SPA, Nguyen-Xuan H, Vo TP. Isogeometric analysis for functionally graded microplates based on modified couple stress theory. Comput Methods Appl Math 2016;313. https://doi.org/10.1016/j.cma.2016.10.002.
[83] Thai HT, Kim SE. A size-dependent functionally graded Reddy plate model based on a modified couple stress theory. Compos B Eng 2013;45(1):1636–45. https://doi.org/10.1016/j.compositesb.2012.09.065.
[84] Hosseini-Hashemi S, Karimi M, Rokni H. Natural frequencies of rectangular Mindlin plates coupled with stationary fluid. Appl Math Model 2012;36(2):764–78. https://doi.org/10.1016/j.apm.2011.07.007.